

University of Windsor

Scholarship at UWindor

Major Papers

Theses, Dissertations, and Major Papers

July 2024

Simulation of Delta Winglets to Improve Heat Transfer in Solar Air Heaters

mehrnaz mehdizadeh farsangi

University of Windsor, mehdiza@uwindsor.ca

Follow this and additional works at: <https://scholar.uwindsor.ca/major-papers>



Part of the [Heat Transfer, Combustion Commons](#)

Recommended Citation

mehdizadeh farsangi, mehnaz, "Simulation of Delta Winglets to Improve Heat Transfer in Solar Air Heaters" (2024). *Major Papers*. 309.

<https://scholar.uwindsor.ca/major-papers/309>

This Major Research Paper is brought to you for free and open access by the Theses, Dissertations, and Major Papers at Scholarship at UWindor. It has been accepted for inclusion in Major Papers by an authorized administrator of Scholarship at UWindor. For more information, please contact scholarship@uwindsor.ca.

Simulation of Delta Winglets to Improve Heat Transfer in Solar Air Heaters

by

Mehrnaz Mehdizadeh Farsangi

A Major Research Paper

Submitted to the Faculty of Graduate Studies

through the Department of Mechanical, Automotive and Materials

Engineering in Partial Fulfilment of the Requirements

for the Degree of Master of Applied Science at the

University of Windsor

Windsor, Ontario, Canada

@2024 Mehnaz Mehdizadeh Farsangi

Simulation of Delta Winglets to Improve Heat Transfer in Solar Air Heaters

By

Mehrnaz Mehdizadeh Farsangi

APPROVED BY:

J. Stagner

Department of Mechanical, Automotive and Materials Engineering

P. Henshaw, Co-Advisor

Department of Civil and Environmental Engineering

O. Jianu, Co-Advisor

Department of Mechanical, Automotive and Materials Engineering

June 13, 2024

Declaration of co-authorship

Co-Authorship

I hereby declare that this major research paper incorporates material that is the result of joint research. This major research paper incorporates the outcome of joint research undertaken under the supervision of Dr. Paul Henshaw. In all cases, the key ideas, primary contributions, data analysis and interpretation, were performed by the author, and the contribution of the co-author was primarily through feedback corrections, improvement of ideas and editing the manuscript.

I am aware of the University of Windsor Senate Policy on Authorship, and I certify that I have properly acknowledged the contribution of other researchers to my major research paper and have obtained written permission from each of the co-author(s) to include the above material(s) in my major research paper. I certify that, with the above qualification, this major research paper, and the research to which it refers, is the product of my own work.

General

I declare that, to the best of my knowledge, my major research paper does not infringe upon anyone's copyright nor violate any proprietary rights and that any ideas, techniques, quotations, or any other material from the work of other people included in my major research paper, published or otherwise, are fully acknowledged in accordance with the standard referencing practices. Furthermore, to the extent that I have included copyrighted material that surpasses the

bounds of fair dealing within the meaning of the Canada Copyright Act, I certify that I have obtained a written permission from the copyright owner(s) to include such material(s) in my major paper. I declare that this is a true copy of my major research paper, including any final revisions, as approved by my major research paper committee and the Graduate Studies office, and that this major research paper has not been submitted for a higher degree to any other University or Institution.

Abstract

Solar air heaters (SAHs) offer a sustainable energy solution, but their efficiency in using solar radiation to heat air can be further optimized. Delta winglet vortex generators (WVG) have proven effective in enhancing heat transfer from the SAH absorber plate to the air passing through the SAH, yet a comprehensive understanding of how different WVG arrangements impact both heat transfer and pressure drop is lacking. This research investigates pairs of WVGs in a common flow-up arrangement at various attack angles and Reynolds numbers (Re), aiming to bridge this knowledge gap and guide the improvement of SAH design.

Numerical simulations were conducted using ANSYS FLUENT 2023R2, with the model verified through a mesh independence study followed by comparison to a smooth duct and common flow-down simulations. The simulations employed a 3D, incompressible, steady-state flow model with the RNG $k-\epsilon$ turbulence model for accurate representation of airflow within the SAH.

Key findings demonstrate that the Nusselt Number (Nu) increases with the Re for the common flow-up WVG arrangement. Furthermore, Nu initially increases with an attack angle from 30° to 60° before decreasing from 60° to 90° for $Re=3500$ and 6500 . At higher Re ($Re=10000$, 13000 , 16000), the optimal attack angle for maximizing Nu shifts to 45° . The friction factor (f) demonstrates an initial increase as the attack angle rises from 30° to 60° , followed by a decrease as α continues to increase from 60° to 90° . Notably, a maximum thermal efficiency factor (TEF) of 1.7 was achieved at $Re=3500$ and an attack angle of 30° , indicating the potential for significant SAH performance improvement using the common flow-up configuration. However, higher $TEFs$ were reported in the literature using pairs of WVGs in common flow-down configurations. These findings highlight the interplay between geometric parameters and flow conditions, providing valuable insights for optimizing SAH design.

Dedication

To my supportive husband, Ali, whose unwavering encouragement and belief in me made this journey possible.

Table of Contents

Declaration of co-authorship	III
Abstract.....	V
Dedication.....	VI
List of Tables	IX
List of Figures	X
Nomenclature	XI
1. INTRODUCTION	1
1.1 Problem Statement.....	1
1.2 Objectives.....	3
1.3 Major Paper Structure.....	3
2. LITERATURE REVIEW	4
2.1 Introduction to Solar Air Heaters (SAHs).....	4
2.2 Basics of Heat Transfer	4
2.3 Enhancing Heat Transfer in SAHs	6
2.4 CFD in Winglet Research	9
2.5 Research Gap	11
3. METHODOLOGY	12
3.1 Modelling Tools.....	12
3.2 Mesh Size Optimization	14
3.3 Comparison	15
3.3.1 Smooth Duct.....	15
3.3.2 Common Flow-Down Configuration	15
3.4 Application	17
4. RESULTS AND DISCUSSION	19
4.1 Mesh Size Optimization	19

4.2 Comparison to Baseline.....	20
4.3 Application	21
4.4 Nusselt number and friction factor correlations	26
5. CONCLUSION AND FUTURE DIRECTIONS.....	32
5.1 Conclusions.....	32
5.2 Future Research Directions	32
REFERENCES	34
VITA AUCTORIS	38

List of Tables

Table 1. Highlights of studies on effects of turbulent generators on heat transfer	10
Table 2. Winglet Dimensions In the Study.	17

List of Figures

Figure 1. Common Flow-down and Common Flow-up Arrangements of a Pair of Winglets.....	9
Figure 2. Unstructured Mesh Generated on ANSYS	12
Figure 3. Winglet Shape.	16
Figure 4. Depiction of Dimensions Listed in Table 2: a) Transverse Pitch, b) Winglets Gap, c) Longitudinal Pitch.	16
Figure 5. Oblique Diagram of the Arrangement of the Winglets in the SAH.....	17
Figure 6. Front and Top View of Winglets.....	18
Figure 7. Test of Mesh Independency.	19
Figure 8. Smooth Channel Comparison of Nu and f	20
Figure 9. Numerical Result Comparison for Nu and f	21
Figure 10. Flow Pattern Inside the Channel at $Re=3500$ and $\alpha=30^\circ$	22
Figure 11. Details of Streamlines in Different Re	23
Figure 12. Temperature Field of Channel with Common Flow-up Delta Winglet Vortex Generator at $Re=6500$ and $z/L=0.531$	24
Figure 13. Vorticity Contour, for $Re=6500$ at Attack Angles of 30° , 45° , 60° , 75° , 90° and $z/L=0.531$. ..	25
Figure 14. Iso Vortex Downstream of SAH for $Re=6500$, Attack Angle of 60°	26
Figure 15. Predicted Nu and f (Pred) Versus Data from Simulation (Num).....	27
Figure 16. Influence of Angle of Attack on Nu in Different Flow Regimes a) Nusselt Number of the Duct with Winglets, and b) Nusselt Number Scaled to the Case of Smooth Channel.	28
Figure 17. Influence of Angle of Attack on f in Different Flow Regimes a) f of the Duct with Winglets, and b) f Scaled to the Case of Smooth Channel.	29
Figure 18. Influence of α and Re on Thermal Efficiency Factor.	30

Nomenclature

A	absorber plate surface area, m^2
a	height of WVG, m
b	length of WVG, m
C_p	specific heat of fluid, $J \cdot kg^{-1} K^{-1}$
D	duct hydraulic diameter, m
f	friction factor
H	duct height, m
h	heat transfer coefficient, $W \cdot m^{-2} \cdot K^{-1}$
i, j	Cartesian coordinates in x and y direction
K	turbulent kinetic energy, $m^2 \cdot s^{-2}$
L	length of test section, m
Nu	Nusselt number
P	fluid pressure, Pa
Pr	Prandtl number
Re	Reynolds number
SAH	solar air heater
TEF	thermal enhancement factor
u	fluid velocity in the duct, $m \cdot s^{-1}$
WVG	winglet vortex generator

α	flow angle of attack, degrees
ΔP	pressure drop across duct, Pa
ε	dissipation rate, $m^2 \cdot s^{-3}$
σ	winglet aspect ratio
Nu_x	local Nusselt number
T	fluid temperature, K
δ	leading edge tip spacing between WVG pair, m
λ	thermal conductivity of fluid, $W \cdot m^{-1} \cdot K^{-1}$
μ	dynamic viscosity, $kg \cdot s^{-1} \cdot m^{-1}$
ρ	density of fluid, $kg \cdot m^{-3}$
$\frac{P_T}{b}$	relative transverse pitch
$\frac{p_L}{a}$	relative longitudinal pitch
h_x	local heat transfer coefficient, $W \cdot m^{-2} \cdot K^{-1}$
G_k	generation of turbulence kinetic energy due to the mean velocity gradients
$\frac{Nu}{Nu_S}$	Nusselt number ratio
T_f	mean fluid temperature, K
T_w	mean wall temperature, K
$\frac{f}{f_s}$	friction factor ratio
\dot{q}	heat flux, W/m ²

u_i velocity component in x_i direction, m/s

μ_t turbulent viscosity, $kg \cdot s^{-1} \cdot m^{-1}$

σ_k turbulent Prandtl number for k

σ_ε turbulent Prandtl number for ε

1. INTRODUCTION

1.1 Problem Statement

Population growth and industrial development have increased energy needs. The countries of the world depend on fossil fuels, which are limited and finite, to meet their energy requirements. In addition, most of the oil and gas resources are in a small group of countries, which is a threat to energy security for others. Fossil fuels have destructive effects on the environment due to the local pollution caused by their consumption and in extraction phase. Global warming, a serious threat to the planet, is mainly the result of burning fossil fuels to produce energy, which in turn release greenhouse gases into the atmosphere. Also, due to the ever-increasing need of humankind for energy and since fossil fuels are nonrenewable, the energy needs of future generations are compromised. Finally, non-renewable energy sources are not available in all countries. Such limitations caused humans to think about energy supply through renewable sources to protect the environment, provide energy security and maintain the economic growth of the world, which is loosely dependent on energy supply. One of the most important proposed solutions is the investment and development of new and renewable energy technologies such as solar energy, wind energy, biomass, and sea waves. In addition, the increase in the price of fossil fuels and the risk of running out of this type of energy source has become a global concern. Considering the limitation of fossil fuel resources and the harmfulness of unprincipled use of such fuels for the health of the environment, research and applications of renewable energy have become especially important in industrial and scientific societies [1]. Among renewable energies, solar energy can meet thermal and electrical needs and is accessible to many parts of the world. Solar radiation, which is freely available, provides a source of pollution-free and unlimited energy [1]. Environmental friendliness, accessibility, reduced electricity costs, absence of noise, low maintenance cost and advancing technology are among the advantages of this energy. Every day, a large amount of solar energy hits the earth's surface. This energy can be converted to useful heat, or it may be converted directly into electricity using photovoltaic panels. Intermittency, expensive storage, pollution of some materials used in the construction process, need for rare materials, and need for space are among the disadvantages of solar energy.

The easiest way to use solar energy is in heating applications, where solar energy is converted into thermal energy in solar collectors. In terms of heating, there are two types of solar heaters: air and water. Solar air heaters (SAH) are less complicated than solar water heaters as they are easier to make and install and are made with inexpensive materials. These types of heaters are used in indoor space heating as well as in industry and agriculture as dryers. SAH collectors do

not have environmental and noise pollution, and in addition, they do not have moving parts. High lifespan and low maintenance cost are other features of SAHs.

Traditional SAHs mainly include panels (solar collectors) with an integral hot air channel and air blowers in an active system, and without blowers in a passive system. The panels include an absorber plate and one or two transparent covers so that solar radiation can penetrate through to the absorber where solar radiation is absorbed by the absorber plate. The heat absorbed by the absorber is transferred to the air because the air passing through the channel is at a lower temperature than the absorber plate. This heated air can be used for space heating, drying wood and lumber, processing of industrial products, processing of concrete and building components, drying of vegetables, fruits, meats, incubation, and other industrial purposes. Also, these heaters can be combined with photovoltaic systems for the simultaneous production of electricity and heat [2,3].

Unfortunately, despite the benefits and applications of SAHs, their thermal efficiency is low. One reason for this is the low convection heat transfer coefficient between the absorbent plate and the flowing air. This low heat transfer causes the temperature of the absorber to remain high, resulting in a large loss of energy to the environment and a decrease in the efficiency of the collector. The importance of increasing heat transfer can be influential in reducing the energy required for pumping, increasing thermal efficiency, increasing the life of equipment, reducing environmental pollution. Hence, optimizing heat transfer processes becomes crucial for maximizing energy efficiency and minimizing overall energy consumption. The science of heat transfer examines the thermal energy flow between two objects or between two points of the same object that occurs due to their temperature difference. In the science of heat transfer, the first and second laws of thermodynamics are observed together with empirical correlations, to obtain the rate of thermal energy flow (heat transfer). Heat transfer takes place in three ways: conduction, convection, and radiation [4].

To improve the heat transfer in solar air heaters, different flow regimes have been created using porosity and artificial roughness [5]. In some cases, the artificial roughness has taken the form of fins, twisted strips, baffles, or winglets on the absorber plate to increase the convection coefficient of the absorber [2]. Also, creating an artificial roughness on the surface of the absorber with a thickness of a smooth substrate [6] to make it turbulent with the minimum possible pressure drop, as well as using a porous medium in the solar air heater channel [7] have been investigated. In addition to the mentioned cases, reducing the heat losses of the system by double walling the glass cover [8] or using selective coating on the absorber to influence the radiation properties of the absorber and as a result reduce the radiant heat losses and increase the efficiency of the system are also other methods that have been presented [9].

Winglets are devices that are installed perpendicular to the surface and boost the effects of created vortices by creating turbulence in the air flow. The most important point in the design of winglets are their geometric characteristics and the angle of their placement relative to the airflow, which can lead to an increase in the heat transfer coefficient of the surface [10]. Winglets create longitudinal swirling currents to increase the heat transfer coefficient, but they also increase the effective friction coefficient. Hence, the use of winglets to disturb the flow could increase heat transfer in the SAH [11,12]. However, the most important challenge and issue in increasing the thermal efficiency of SAHs is having a minimal increase in the pressure drop in the solar air heater channel while enhancing the heat transfer rate. Overcoming this challenge is considered as the main idea of this research, which provides the motivation of doing this study.

1.2 Objectives

The main goal of the research is increasing the efficiency of a flat-plate solar air heater by installing winglets on the surface. To achieve this goal the study of heat transfer and friction for delta winglets in flowing air at various attack angles ($30^\circ, 45^\circ, 60^\circ, 75^\circ, 90^\circ$) and Re (3500, 6500, 10000, 13000, 16000) has been simulated using computational fluid dynamics.

1.3 Major Paper Structure

This research has been compiled in the form of five chapters. In the first chapter, the generalities of the research, including the problem statement, the importance motivation of the research, objectives, and research questions are discussed so that the reader would be informed about the nature of this research and its direction. In the second chapter, the theoretical foundations are examined, the definitions of concepts related to SAHs, basics of heat transfer, types of solar panels, winglets, and their role in increasing the efficiency of heat transfer of air-heating solar panels and all the necessary items for explanation and study related to the subject will be presented based on a literature review. In the third chapter, the steps of the proposed research method are presented. In the fourth chapter, analysis of the data obtained from the application of the proposed method is presented. In the fifth chapter, conclusions and future practical suggestions are presented.

2. LITERATURE REVIEW

2.1 Introduction to Solar Air Heaters (SAHs)

SAHs are integral elements within some solar thermal energy systems, cleverly designed to transform incident solar radiation into usable thermal energy for the purpose of raising air temperatures. This energy is then transferred to the air, elevating its temperature. Beyond their immediate thermal benefits, SAHs contribute significantly to environmental sustainability. By displacing traditional fossil-fuel-based heating, they play a role in lowering greenhouse gas emissions. Mushatet and Bader demonstrated the potential of SAHs in industrial applications [13]. Tiwari demonstrated a successful case study of SAH integration in a greenhouse, significantly reducing heating costs [14].

Pioneering studies on SAH emerged in the mid-20th century, notably the work by Hottel and Woertz [15]. Kalogirou's comprehensive study [16] elucidates the interplay of conduction, convection, and radiation in solar air heaters (SAHs), revealing their relative contributions to overall thermal performance.

Subsequent advances in materials science, particularly the development of efficient absorber coatings, significantly enhanced SAH performance. Duffie and Beckman [17] provide a comprehensive review of advancements in materials science, particularly the development of efficient absorber coatings, which have significantly enhanced SAH performance. These advancements have paved the way for progressively more sophisticated SAH designs over the past several decades. For instance, Karim and Hawlader [18] developed V-groove solar air collectors, demonstrating the ongoing technological refinements in this field. Their design aimed to increase the surface area of the absorber, thereby improving heat transfer efficiency.

2.2 Basics of Heat Transfer

Heat transfer lies at the heart of SAH functionality and understanding conduction, radiation and convection are essential.

Conduction involves the transfer of heat through a solid material. In SAHs, conduction is critical for heat transfer within the absorber plate itself. Material choice and thickness influence thermal conductivity, and Fourier's Law (Eq. 1) helps quantify this process:

$$\dot{Q} = -\frac{kA\Delta T}{\Delta x} \quad (1)$$

Where k is thermal conductivity of the material (W/m·K), and Δx is thickness of the absorber plate(m).

In convection mode, heat moves with a fluid (like air). SAHs rely heavily on convection to transfer heat from the absorber plate to the flowing air. Optimizing airflow patterns is crucial for maximizing convective heat transfer efficiency. Additionally, the equation used to calculate the heat transfer coefficient (h) between the absorber plate and the flowing fluid will be defined:

$$\dot{Q} = hA(T_{\omega} - T_f) \quad (2)$$

where T_{ω} is the absorber plate temperature (°C or K).

The mean bulk fluid temperature (T_f) is determined by integrating the temperature of the fluid adjacent to the absorber plate, over the absorber plate area [19]:

$$T_f = \frac{\int T u \rho dA}{\int u \rho dA} \quad (3)$$

where T is local temperature at a point on the absorber plate (°C or K), u is the local flow velocity (m/s), ρ is fluid density (kg/m³) and A is absorber plate surface area (m²).

Nusselt number is a dimensionless parameter that characterizes the efficiency of convective heat transfer in SAHs. A higher Nu shows greater heat transfer potential. SAH designs often aim to maximize the Nu by optimizing air flow patterns and surface geometries.

The local Nu (Nu_x) is shown as:

$$Nu_x = \frac{h_x D}{k} \quad (4)$$

where h_x is the convection heat transfer coefficient at a distance x from the leading edge of the absorber plate(W/m²·K), k is thermal conductivity of the fluid (W/m·K), and D is the hydraulic diameter (m).

By integrating the local Nusselt number over the absorber plate surface, one can determine the average Nusselt number (Nu):

$$Nu = \frac{1}{A} \int Nu_x dA \quad (5)$$

The friction factor (f), representing the energy required to move the air through the channel, is calculated by:

$$f = \frac{\Delta P}{\left(\frac{L}{D}\right) \left(\rho \frac{u_m^2}{2}\right)} \quad (6)$$

where ΔP is defined as the pressure drop across the channel (Pa), L is the length of the channel (m), D is the hydraulic diameter(m), u_m is the mean flow velocity(m/s), and ρ is the density of the fluid (kg/m³).

The thermal enhancement factor (TEF), a measure of overall thermohydraulic performance, is defined as [36]:

$$TEF = \frac{Nu/Nu_s}{\left(\frac{f}{f_s}\right)^{\frac{1}{3}}} \quad (7)$$

where Nu is the average Nu with vortex generators, Nu_s is the average Nu in a smooth channel, f is the friction factor with vortex turbulence generators, and f_s is the friction factor in a smooth channel.

2.3 Enhancing Heat Transfer in SAHs

To maximize heat transfer rates and enhance the efficiency of SAHs, researchers have explored various techniques, including the incorporation of turbulent promoters on heat transfer surfaces. Among these techniques, the use of artificial roughness, such as ribs, fins, baffles, and winglets, has shown promise in augmenting convective heat transfer [19]. Specifically, winglets have gained attention for their ability to induce vortices and enhance fluid mixing, thereby improving heat transfer characteristics within SAH ducts.

One strategy involves directly incorporating structures onto the SAH absorber plate. Bekele et al. [20] found success using winglets, reporting an enhancement in the Nu of about 3.5 times

compared to a smooth plate design. Kumar et al. [21] investigated the use of multi-V-shaped ribs with gaps on the absorber plate of a solar air heater, finding that this configuration could significantly enhance heat transfer compared to a smooth plate. Pandey et al. [22] explored the use of multiple arcs with gaps on the absorber plate and observed improved heat transfer performance. Tamna et al. [23] studied V-baffle vortex generators in a solar air heater channel and found that they could generate multiple longitudinal vortex flows, leading to increased turbulence intensity and better mixing of the fluid, thereby enhancing heat transfer. Skullong et al. [24] combined wavy grooves with perforated delta-wing vortex generators and demonstrated the potential of using multiple techniques together to achieve even greater heat transfer enhancement in solar air heaters.

Winglets, strategically shaped protrusions added to the absorber plate of solar air heaters, can play a significant role in boosting thermal efficiency. Primarily, they function by disrupting the laminar airflow within the SAH duct. The boundary layer is a region where heat transfer is naturally less efficient as it acts like a barrier for fluid movement. Anything that promotes turbulent flow disrupts the boundary layer that forms near the heated absorber surface. Essentially winglets facilitate mixing between the cooler incoming air and the heated surface, enhancing convective heat transfer. Additionally, metal winglets increase the effective surface area of the absorber plate, providing more space for this heat exchange to occur. Certain winglet configurations can even induce the formation of longitudinal vortices, which further augment heat transfer while potentially mitigating pressure drop by re-energizing the boundary layer [25].

The effectiveness of winglets depends on various factors, including their specific size, shape, placement on the absorber plate, and the angle of attack relative to the incoming airflow. Research by Kumar and Goel [26] demonstrates how strategically designed winglets can significantly enhance heat transfer efficiency in SAHs, particularly when considering the interplay between airflow characteristics and winglet design. Furthermore, studies by Promvonge et al. [27] and Skullong et al. [24] reinforce the importance of both winglet geometry and airflow characteristics in influencing the overall performance improvement of SAHs. Research has actively explored how heat transfer enhancement techniques can be adapted to various SAH geometries. Hiravennavar et al. [28] and Althaher et al. [29] demonstrated the successful application of vortex generators within triangular ducts.

Delta winglet vortex generators employ triangular blades in the airstream, where the plane of the blade is perpendicular to the surface to which it is attached, and one side of the triangle is adjacent to the surface. The plane of the winglets is often at an angle to the direction of the bulk flow,

referred to as “angle of attack”. Delta winglet vortex generators have received substantial attention in SAH research. Tang et al. [30] specifically tailored their winglet longitudinal vortex generator design for rectangular SAH channels. Wijayanta et al. [5] further demonstrated the versatility of delta winglet vortex generators by extending their implementation to a double-pipe heat exchanger.

Multiple winglets can be arranged in parallel so that they have the same angle of attack. As per Figure 1, delta WVGs can also be arranged in pairs such that one winglet of each pair has a positive angle of attack and the other has a negative angle of attack, in which case the pairs can be either “common flow-down”, where an apex of the triangle is at the furthest upstream point of the winglet, or “common flow-up” where an apex is at the furthest downstream point of the winglet. In both cases, the apexes mentioned are the closest points of each pair of winglets. Wu et al. [31] focused on the impact of the delta winglet angle of attack on heat transfer performance, while Mohanakrishnan et al. [10] investigated the critical importance of optimizing transverse spacing between winglets. These studies showcase the importance of careful geometric configuration, even within the promising delta winglet category.

While winglets offer significant gains in heat transfer, it is important to be mindful of their potential downside. The very features that disrupt airflow and enhance heat transfer can also lead to an increase in pressure drop across the SAH system. Increased pressure drop means that more energy must be expended to force air through the channel containing the winglets, to maintain the same velocity. Therefore, a careful balance is needed to maximize thermal efficiency while managing this potential drawback. Studies by Caliskan [32] emphasize the crucial balance between heat transfer enhancement and pressure drop when incorporating winglets into SAH designs. Studies by Karwa and Maheshwari [33], Skullong and Promvonge [34], and Wijayanta et al. [5] highlight the need to meticulously balance the benefits of improved heat transfer against this potential drawback. Certain designs, like delta wing pairs, can induce vortices that enhance heat transfer while potentially mitigating pressure drop [32]. Min and Zhang [35] specifically focus on numerical methods for analyzing and optimizing winglet configurations.

The shape and size of vortex generators play a significant role in their effectiveness. Chamoli et al. [19] investigated the thermal performance of a solar air heater with winglet vortex generators, examining how the shape and arrangement of the winglets affected heat transfer. They found that the winglets could significantly improve the heater's efficiency. Alam and Kim [36] used numerical simulations to study a solar air heater duct with semi-elliptical obstacles. They focused on how the shape and arrangement of these obstacles impacted both heat transfer and friction

characteristics. Min and Zhang [35] explored how delta winglets could enhance convective mass transfer in a membrane channel. They compared delta winglets to rectangular ones and analyzed how the shape of the winglet affected mass transfer efficiency.

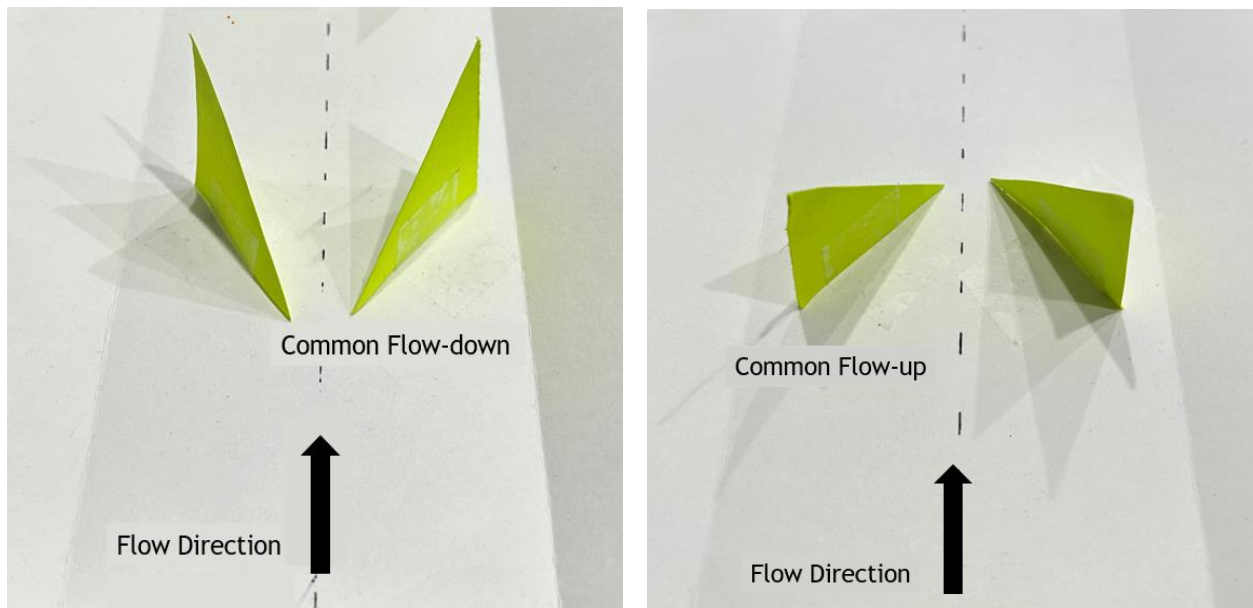


Figure 1. Common Flow-down and Common Flow-up Arrangements of a Pair of Winglets.

2.4 CFD in Winglet Research

Computational Fluid Dynamics (CFD) emerges as a powerful tool for analyzing and enhancing winglet performance in solar air heaters. This technique allows for simulating complex airflow patterns around winglets, providing insights into phenomena such as boundary layer disruption, turbulence, and vortex formation [5]. Furthermore, CFD simulations can predict temperature distributions within the SAH and quantify the impact of winglets on heat transfer efficiency, as demonstrated by Chamoli et al. [19]. This enables researchers to optimize winglet parameters (size, shape, angle of attack, spacing) for maximum efficiency, reducing reliance on physical prototyping.

Experimental studies are critical for validating theoretical concepts and CFD predictions. Wind tunnel experiments offer a complementary approach to analyzing winglet performance in solar air heaters. These tests enable researchers to measure temperature profiles and pressure differences across systems with and without winglets, quantifying the impact on heat transfer

coefficients and energy gains [37]. Additionally, wind tunnel studies can identify potential increases in pressure drop due to winglet implementation. Promvong and Skullong [24] conducted a comprehensive wind tunnel investigation, exploring a wide range of winglet configurations and their effects on SAH performance, providing valuable experimental data for design optimization. By combining these experimental insights with theoretical and CFD models, researchers can develop a holistic understanding of winglet design, ultimately leading to advancements in SAH thermal efficiency.

The extensive body of research reviewed here confirms the significant potential of using both obstacles and vortex generators to improve solar air heater performance. This research has been summarized in Table 1 Delta winglet vortex generators emerge as a promising technique. Ongoing research into optimizing the shape, size, placement, and combination of these various strategies offers the potential for even greater gains in heat transfer efficiency. Future advancements in SAH design must carefully consider the balance between these improvements and any associated increases in pressure loss.

Table 1. Highlights of studies on effects of turbulent generators on heat transfer

Study	Studied Configuration	Major Findings
21	Multi V-shaped ribs with gaps in rectangular ducts, varied rib geometry, Re range.	Significant heat transfer increase (up to 6.74 times) but also increased friction (up to 6.37 times). Optimal rib configuration identified.
23	V-baffle vortex generators in solar air heater channel. Varied baffle pitch, arrangement. Re range.	Significant heat transfer increase. Smaller baffle pitch leads to higher friction. Single baffle with specific pitch offers best thermal performance.
24	In the SAH, combined wavy-groove and delta-wing vortex generators (WVGs). varying Re , porosity, and spacing of WVG.	Significant heat transfer increase with friction increase. Optimal combination of WVG porosity and spacing exists for best thermal performance.
36	Novel winglet LVG configurations with elliptical poles for rectangular channels.	New configurations significantly enhance heat transfer. Case F (delta winglet + elliptical pole) offers the best overall performance based on field synergy principle and JF factor analysis.
33	Rectangular duct with fully/half-perforated baffles on one wall (simulating solar air heater). Varied baffle pitch, fixed Re .	Both baffle types enhance heat transfer but increase friction. Half-perforated baffles are thermohydraulically superior. Best configuration: half-perforated, pitch of 7.2 for maximum performance at the same pumping power.
5	A double-pipe heat exchanger with double-sided delta-wing (T-W) tape inserts. constant Re and variable wing-width ratio.	Significant heat transfer enhancement, highest with widest wing-width ratio. Increased friction factor. Thermal performance factor improves, maximized with widest wing-width ratio. Empirical correlations developed

31	Single delta winglet on a flat plate. Varied attack angle, fixed Re .	Heat transfer increases with attack angle. Sharp enhancement near the winglet (transverse vortex), gradual enhancement further downstream (longitudinal vortices). Attack angle influences vortex strength and thus the degree of heat transfer improvement.
10	Delta winglet pair in front of a solar panel. Varied transverse spacing, fixed Re and winglet geometry.	Spacing of 2 winglet heights produced the greatest heat transfer increase. Vortical flow structures (especially downwash) play a crucial role in the enhancement mechanism.
19,36,35	Winglet vortex generator (WVG) in solar air heater. Varied WVG tip edge ratio and angle of attack, fixed Re . Numerical simulation.	Highest heat transfer and friction at $\alpha=60^\circ$ and $c/a=1$ (full tip edge). Best thermal performance (TEF) at $\alpha=30^\circ$ and $c/a=0$ (no tip edge), TEF range 1.72-2.20. WVG configuration impacts flow/temperature fields, influencing heat transfer and friction.

2.5 Research Gap

While extensive research has established the effectiveness of delta winglet vortex generators in enhancing heat transfer compared to other types, a knowledge gap exists regarding the influence of various multiple delta winglet arrangements on both heat transfer and pressure drop characteristics. Existing studies have primarily focused on common flow-down and flow-up configurations at varying Re and attack angles. Each configuration induces a different flow pattern and vortex interaction within the SAH. For instance, Chamoli et al. [19] investigated the impact of common flow-down configuration at different Re and attack angles. Similarly, Ke et al. [38] compared the performance of common flow-up and flow-down configurations, but with a fixed attack angle of 45° .

This research aims to address this gap by exploring the effects of multiple winglet common flow-up arrangements at untested attack angles and Re values. Initially, a SAH duct model without winglets and a multiple-winglet common flow-down model were simulated to determine the baseline performance of SAH. Then a common flow-up model was simulated with different attack angles. By analyzing these previously unconsidered configurations and comparing the results to those of smooth channels and Chamoli et al.'s [19] findings, this study seeks to contribute valuable insights into the performance of delta winglets for SAHs.

3. METHODOLOGY

This chapter details the development and validation of a numerical model utilized to investigate the effects of a common flow-up delta winglet arrangement at various attack angles and Reynolds numbers on solar air heater performance.

3.1 Modelling Tools

The commercial software ANSYS FLUENT 2023R2 (Canonsburg, Pennsylvania) was employed for both model development and subsequent numerical simulations. The simulations assumed a three-dimensional (3D), incompressible, and steady-state flow regime. The RNG k- ϵ turbulence model with enhanced wall treatment was chosen to account for the turbulent nature of the airflow within the SAH. ANSYS's capabilities are used to create an unstructured mesh (Figure 2), emphasizing refinement near the walls and winglets using prism layers to accurately capture boundary layer phenomena. The air flow is in the z-direction along the rectangular duct, with the top surface of the duct representing the hot absorber. Simulations are run until residuals meet the following thresholds: velocities ($<10^{-5}$), continuity ($<10^{-4}$), turbulence kinetic energy and dissipation rate ($<10^{-4}$), and energy ($<10^{-7}$). These thresholds were chosen to align with the study by Chamoli et al. [19].

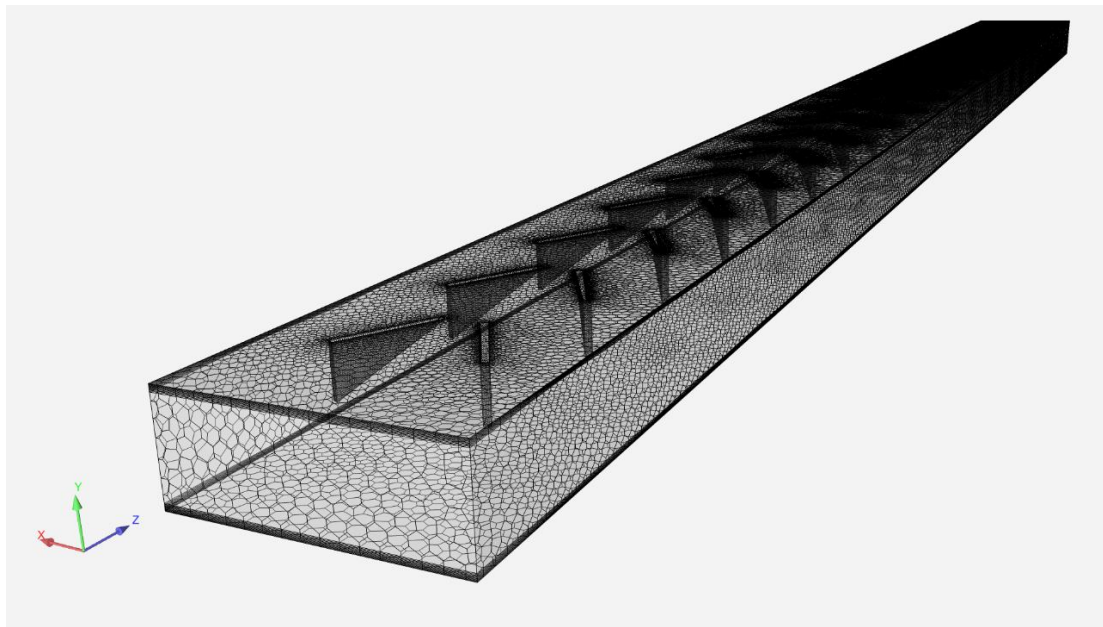


Figure 2. Unstructured Mesh Generated on ANSYS

The equations to be solved include [19]:

Continuity:

$$\frac{\partial}{\partial x_i}(\rho u_i) = 0 \quad (9)$$

Momentum:

$$\frac{\partial}{\partial x_j}(\rho \overline{u_i u_j}) = -\frac{\partial p}{\partial x_i} + \frac{\partial}{\partial x_j} \left(\mu \left(\frac{\partial u_i}{\partial x_j} + \frac{\partial u_j}{\partial x_i} \right) \right) - \frac{\partial(\rho \overline{u'_i u'_j})}{\partial x_j} \quad (10)$$

Energy

$$\frac{\partial}{\partial x_j}(\rho u_j (\rho e + p)) = \frac{\partial}{\partial x_j} \left(\lambda \frac{\partial T}{\partial x_j} \right) \quad (11)$$

Turbulence kinetic energy

$$\frac{\partial}{\partial x_j}(\rho k u_j) = \frac{\partial}{\partial x_j} \left(\left(\mu + \frac{\mu_t}{\sigma_k} \right) \lambda \frac{\partial k}{\partial x_j} \right) + G_k - \rho \varepsilon \quad (12)$$

Turbulence dissipation rate

$$\frac{\partial}{\partial x_j}(\rho \varepsilon u_j) = \frac{\partial}{\partial x_j} \left(\left(\mu + \frac{\mu_t}{\sigma_\varepsilon} \right) \lambda \frac{\partial \varepsilon}{\partial x_j} \right) + C_{1\varepsilon} \frac{\varepsilon}{k} G_k - C_{2\varepsilon} \rho \frac{\varepsilon^2}{k} \quad (13)$$

Air, the working fluid, was modeled with constant properties: Prandtl number $Pr=0.73$, density $\rho=1.1645 \text{ kg/m}^3$, thermal conductivity $\lambda=0.02588 \text{ W/m}\cdot\text{K}$, dynamic viscosity $\mu=1.87 \times 10^{-5} \text{ Pa}\cdot\text{s}$, and specific heat capacity $C_p=1007 \text{ J/kg}\cdot\text{K}$ [19]. The properties remained largely stable across the investigated temperature range [19].

The numerical simulations conducted in this study yielded several key outputs that will be analyzed to evaluate the influence of common flow-up delta winglet vortex generators on SAH performance. These outputs include:

Nu : This dimensionless quantity serves as a crucial indicator of heat transfer performance within the SAH channel. A higher Nu signifies enhanced heat transfer between the airflow and the absorber plate.

Flow Visualization: Visual representations of the flow field will be generated to depict the vortex structures induced by the WVGs. These vortices play a vital role in disrupting the boundary layer near the absorber plate, promoting better heat transfer through increased mixing within the flow.

Friction Factor (f): This parameter reflects the pressure drop experienced by the airflow as it travels through the SAH channel. While essential for understanding the pumping power requirements, a lower friction factor is generally desirable as it minimizes pressure losses.

Thermal Efficiency Factor (TEF): As defined in Chapter 2, the TEF serves as a composite metric that incorporates both heat transfer enhancement (represented by Nu/Nu_s) and pressure drop considerations (represented by f/f_s). A higher TEF signifies a more optimal balance between these competing factors, leading to improved overall SAH performance.

The data obtained from the simulations for Nu , friction factor, and TEF were analyzed across various attack angles and Re . The visualization of the flow field is used to qualitatively assess the influence of WVGs on the flow patterns and boundary layer development within the SAH channel. By integrating these analyses, this study aims to establish a comprehensive understanding of how common flow up WVG arrangements impact SAH performance.

3.2 Mesh Size Optimization

To ensure the accuracy of the simulations, a mesh independence study was conducted for common flow-up configuration, described in Section 3.4. To find an optimal balance between solution accuracy and computational cost, four different mesh sizes were used, which are $E_1 = 1,470,779$, $E_2 = 2,692,013$, $E_3 = 3,889,617$, $E_4 = 5,250,982$. Choosing the optimal initial mesh density requires careful consideration of the geometry's complexity, expected flow behavior, computational limitations, and common practices within the field of research. There is no one-size-fits-all starting mesh size.

Also, the Grid Convergence Index (GCI) which is a method used in Computational Fluid Dynamics (CFD) to estimate the discretization error in simulation results due to the finite size of the computational mesh, is used in this study [40]. It helps assess how much the results would change if a finer mesh were used and determine if the current mesh is sufficiently refined.

The GCI is calculated for each pair of consecutive mesh sizes using the relative error between the results on the two meshes and the apparent order of convergence [40]. A lower GCI indicates that the solution is approaching grid independence.

In this study, a mesh independence study was conducted using four different mesh sizes. The GCI for the Nu and friction factor were calculated using the finest three meshes.

3.3 Comparison

The computational method to simulate the common flow-up winglet configuration in a SAH was first compared with smooth (no winglet) and common flow-down configurations.

3.3.1 Smooth Duct

Since the study focuses on enhancement relative to a smooth channel, a baseline simulation was performed on the duct without winglets. Duct dimensions, governing equations, boundary conditions, and Re were the same as with the winglets. Numerical results for a smooth channel were compared with the established Dittus-Boelter and modified Blasius correlations for Nu and friction factor [20], respectively.

3.3.2 Common Flow-Down Configuration

Also, to ensure the accuracy of the numerical methodology, simulations were conducted with a winglet vortex generator in a SAH duct with common flow-down configuration. The results of these simulations were compared to the numerical study of Chamoli et al. [19] which was validated by the experimental data of Bekele et al. [20]. The simulated SAH has dimensions of 1100 mm x 400 mm x 30 mm, consistent with the model established by Chamoli et al. [19] and Thakur and Chamoli et al. [39]. Delta winglet vortex generators are arranged in pairs, as common flow-down. As suggested by Chamoli et al., a single column of the winglet vortex generator pairs is considered in the numeric study to save computational time. In this simulated channel, sidewall effects on the temperature field and flow are neglected. A uniform heat flux of $1000 \frac{W}{m^2}$ is assumed to originate from the top surface of the duct, which is deemed to be the absorber.

As suggested by Bekele et al. [38] in their experimental set up, natural convection and radiation can be neglected. The bottom of the channel is assumed to be smooth and well insulated. Winglet surfaces and walls are in the no-slip boundary condition. The air entering the SAH already is

assumed to have fully developed flow, minimizing disturbances caused by the entrance, a feature available in ANSYS Fluent.

Due to the strong mixing induced by the vortex generators, the temperature profile also becomes fully developed after a few WVG pairs (approximately 3 or 4) [19]. Thus, any entrance effects on temperature are considered negligible given the total of 20 WVG pairs included in the simulation [28]. The initial air temperature is 300 K.

Following the recommendations of Chamoli et al. [19], Min and Zhang [35] and Skullang and Promvonge [34], the WVGs have a height (a) of 15 mm and a length (b) of 30 mm. The spacing between winglets (δ) is maintained at a gap of 10 mm, with a longitudinal pitch ratio of 3.5 leading to a longitudinal pitch of 52.5 mm and a transverse pitch ratio of 2.67 leading to a transverse pitch of 80.1 mm. The common flow-down configuration was considered for validation to be comparable with Chamoli et al.'s studies.

To maintain consistency with Chamoli et al.'s [19] validated methodology, the full SAH Model is 1100 mm×400 mm×30 mm in which pairs of winglets are at regular z intervals. In real applications, multiple rows and columns of vortex generators can be applied [19]. The simulation incorporates 20 pairs of winglets (40 winglets) along the z -direction. The height (a) and length (b) of the winglet are 15 mm and 30 mm, respectively (Figure 4) as suggested by Min and Zhang [35], Skullang and Promvonge [34], and Chamoli et al [19]. For this study, Re were taken (3500, 6500, 10000, 13000, 16000) and five angles of attack (α) considered (30°, 45°, 60°, 75°, 90°) [19]. Table 2 and Figure 6 show the parameters which were constant in the study.

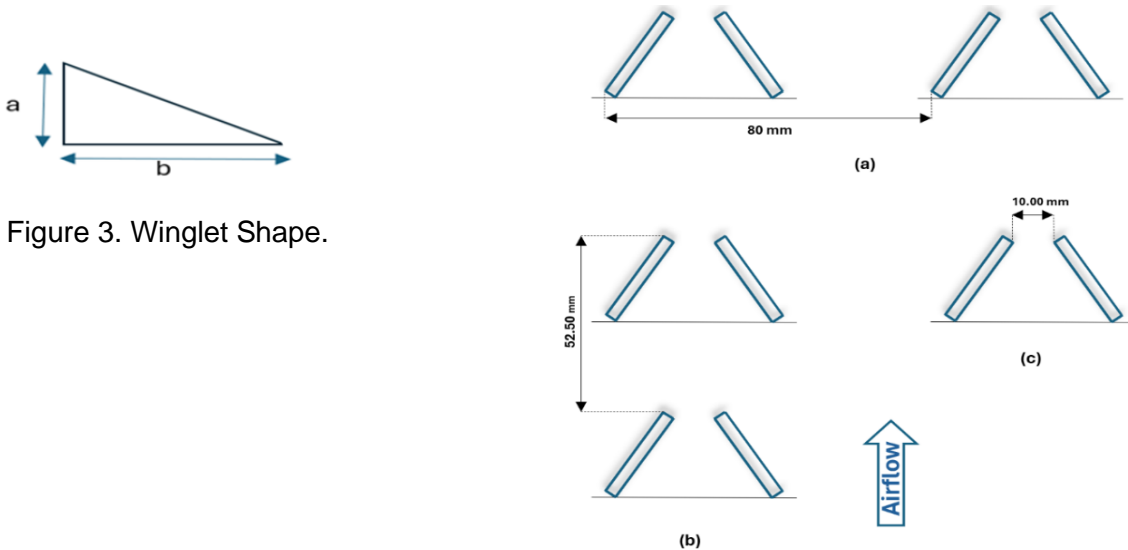


Figure 3. Winglet Shape.

Figure 4. Depiction of Dimensions Listed in Table 2: a) Transverse Pitch, b) Winglets Gap, c) Longitudinal Pitch.

Table 2. Winglet Dimensions In the Study.

Parameter Definition	Dimension (for $a=15$ mm)	Suggested by
Winglet gap (δ)	10 mm	Min et al. [33] Zhou and Ye [41]
Longitudinal pitch ratio $\frac{P_L}{a} = 3.5$	$P_L=52.5$ mm	Bekele et al. [33] Alam and Kim [36]
Transverse pitch ratio $\frac{P_T}{a} = 2.67$	$P_T=80.1$ mm	Bekele et al. [20] Alam and Kim [36]

3.4 Application

For this investigation, the dimensions of the winglets are as mentioned in Chamoli et al [19] and described in Section 3.3.2, but the WVGs are arranged in common flow-up configuration in the SAH as presented in Figures 5 and 6.

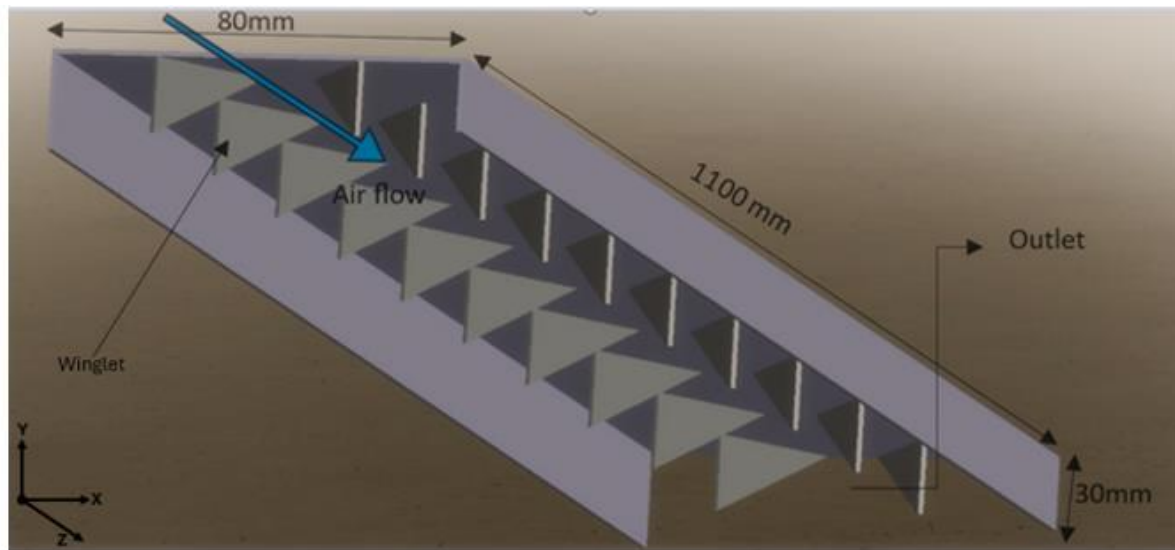


Figure 5. Oblique Diagram of the Arrangement of the Winglets in the SAH.

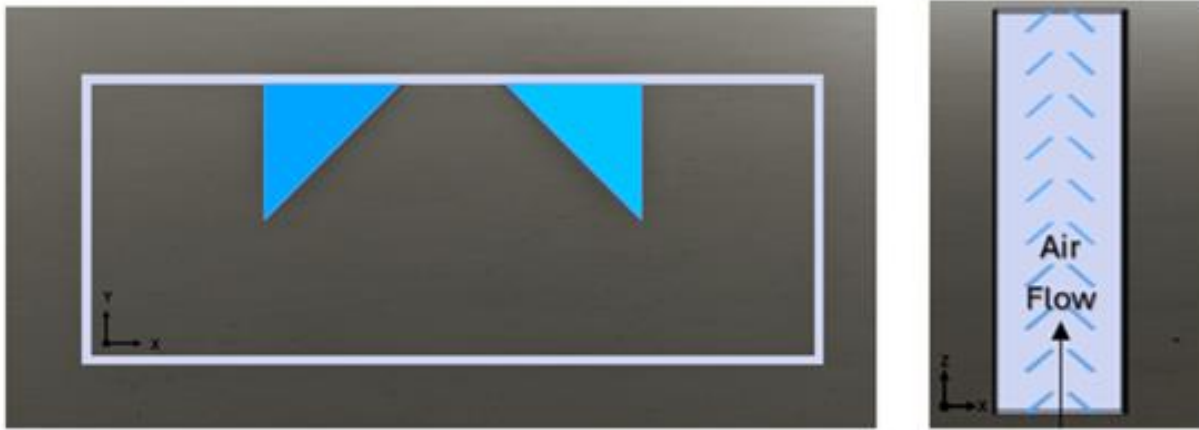


Figure 6. Front and Top View of Winglets.

To enhance visual clarity, Figures 5 and 6 illustrate only 10 pairs of winglets. However, the complete simulation model incorporates 20 pairs along the z-direction.

4. RESULTS AND DISCUSSION

4.1 Mesh Size Optimization

Seeking optimal balance between solution accuracy and computational time, comparison was conducted between four levels. Figure 7 shows that both f and Nu continue to change through level 1 to 2 to 3. The change from level 3 to 4 is negligible (less than 1.75%) and not worth the additional computational effort. It is concluded that ultimately a mesh size of 3,889,617 elements gives the optimal balance between accuracy and computational time chosen for this study.

The GCI for Nu was 0.96%, which is below the desired threshold of 1%, indicating that the solution for Nu is approaching grid independence. The GCI for f was 1.08%, which is slightly above the desired threshold of 1%. However, given the small change in f between the last two mesh levels, it indicates that the results are approaching grid independence. For practical purposes, the chosen mesh size of 3,889,617 elements is considered sufficient for this simulation. The mesh quality was assessed using metrics such as skewness, $y+$, and aspect ratio. The maximum skewness was 0.5, the $y+$ value remained below 5, and the maximum aspect ratio was 1.2. These values indicate a well-structured and high-quality mesh, suitable for accurate CFD simulations.

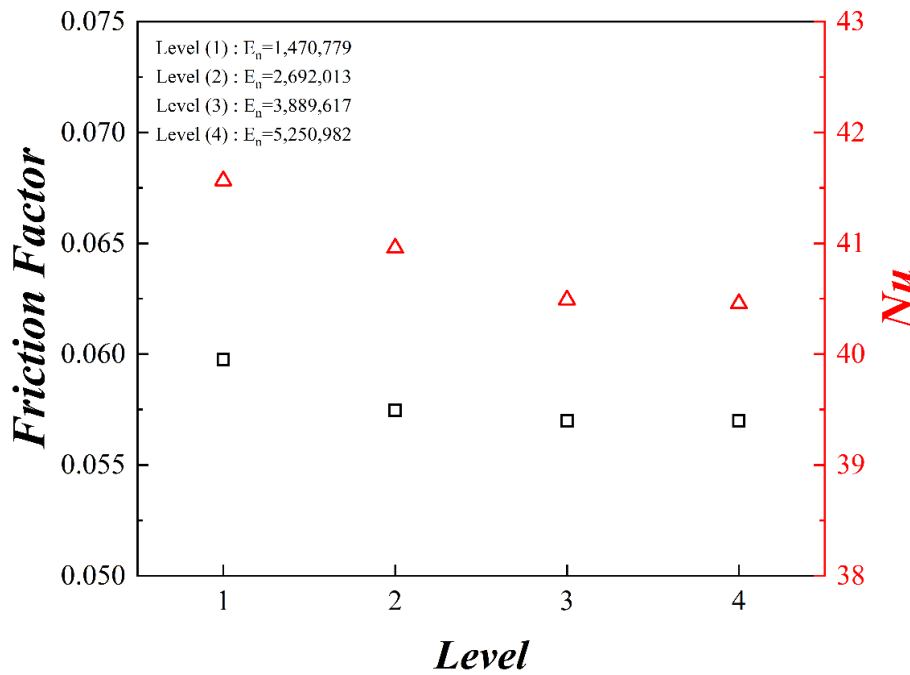


Figure 7. Test of Mesh Independence.

4.2 Comparison to Baseline

When comparing smooth duct simulations to analytical equations and previous experiments, good agreement was found between the ANSYS runs and the theoretical values (Figure 8). Considering theoretical and experimental values, the average absolute deviations of 3.4% for Nu and 8.1% for f were found. However, the results remain slightly lower than the experimental data. Bekele et al. [20] estimated experimental uncertainties of 4.6% for Nu and 1.04% for f . Hence the Nu for the common flow-down configuration is valid. Discrepancies between simulated and experimental results could stem from differences in idealized simulation assumptions versus real-world imperfections, choice of numerical models, and the inherent limitations of experimental measurements. Also, the discrepancy between the present study's results and those of Bekele et al. for the smooth channel, where the present study's values fall outside of Bekele et al.'s reported error bars, could be attributed to the differing treatment of entrance effects. While Bekele et al.'s [20] experimental setup likely included entrance effects, the present numerical model assumes a fully developed flow at the inlet, potentially leading to variations in the calculated Nusselt number and friction factor.

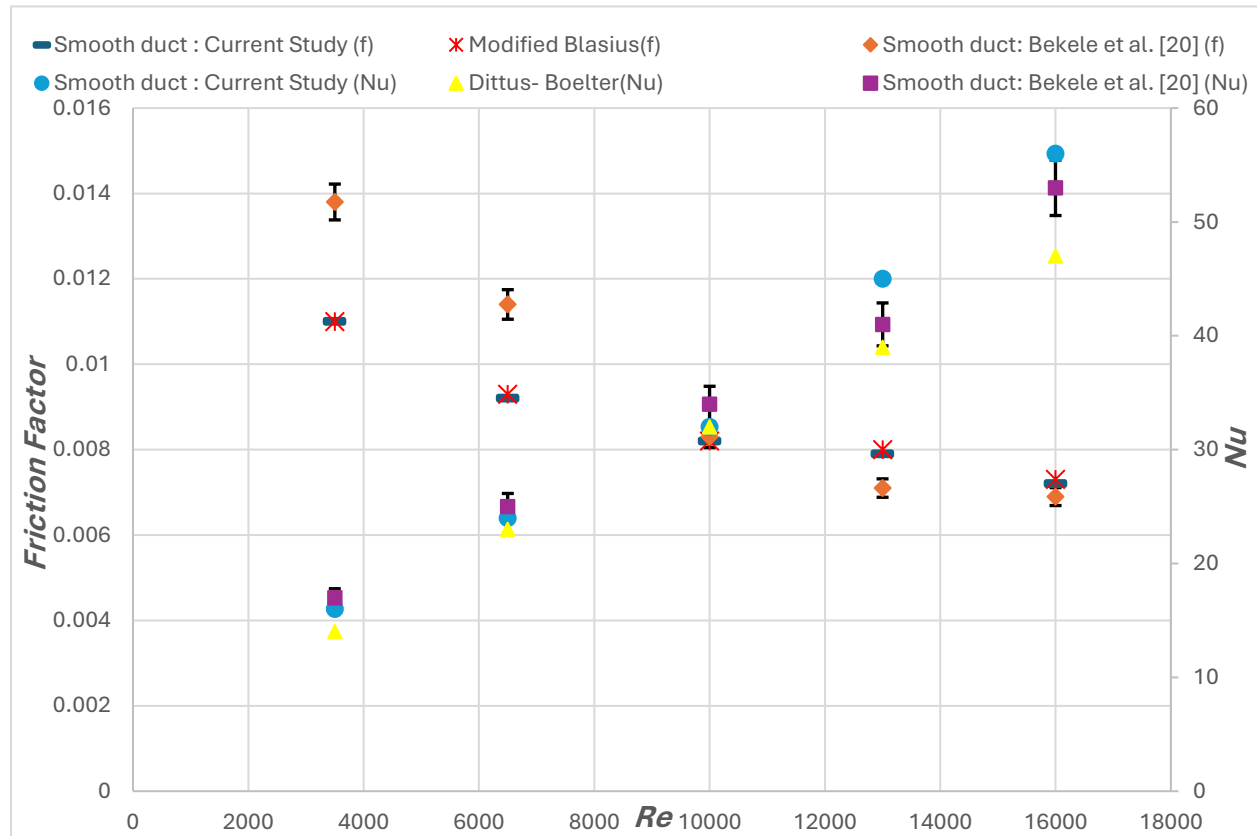


Figure 8. Smooth Channel Comparison of Nu and f .

In comparing the simulation of Chamoli et al.'s common flow-down configuration to reported values, the average absolute deviations were 4.49% for Nu and 9.2% for f from this study, confirming reasonable accuracy and establishing a valid benchmark for subsequent analysis of heat transfer and friction enhancement induced by vortex generators (Figure 9). The present study's results indicate a slightly higher Nu and friction factor compared to Chamoli et al. [19]. While both studies employed the same model, equation solver, turbulence model, minor geometrical variations, boundary condition settings, then potentially even differences in ANSYS versions could contribute to the observed discrepancies.

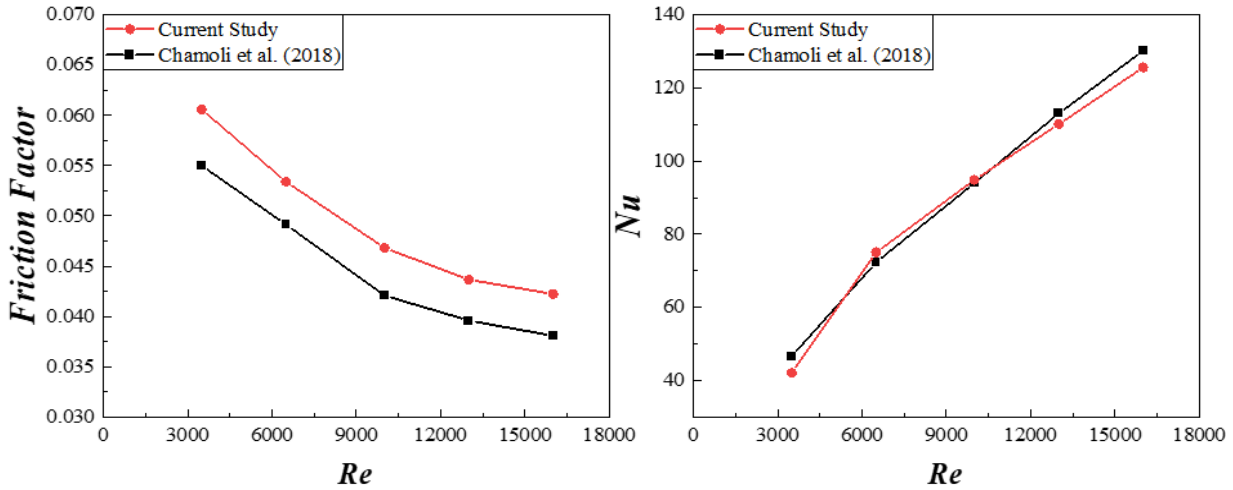


Figure 9. Numerical Result Comparison for Nu and f .

4.3 Application

This section is devoted to discussion of the simulation results for the common flow-up configuration. As it is observed in Figure 10, the flow pattern exhibits a repetitive behavior between consecutive winglets in the flow direction. Therefore, this analysis focuses on the flow characteristics, including transverse streamlines, temperature distribution, and local Nusselt number, within a domain encompassing a pair of winglet vortex generators.

Streamlines depict the path that a massless fluid particle would follow at a given instant in time. They show the direction of the fluid flow at every point in the flow field, where streamlines are closer together, the flow velocity is higher (darker area), while where they are further apart, the flow velocity is lower. Closed or looped streamlines highlight regions where the fluid is swirling or recirculating. Figure 11 clearly demonstrates the impact of delta winglets on the flow pattern within a solar air heater channel across a range of Re ($Re=3500, 6500, 10000, 13000$, and 16000). The white spots at the middle of each item represent the winglets' location. At lower Re values,

indicative of laminar and early transitional flow regimes, the deflection of streamlines around the winglets is more gradual. At higher Re ($Re=10000$, 13000 , 16000), increasing the Re into the turbulent flow regime leads to a significant shift in the flow pattern around the winglets. Streamlines exhibit a sharper deflection, indicating the formation of stronger and larger vortices. The streamlines do not smoothly curve around the winglets. Instead, they make a quick, sharp turn near the front (leading edge) of the winglets. As the streamlines bend, they group up closer together compared to the straighter sections further away. This grouping indicates the flow being squeezed and turning more sharply. These vortices enhance flow mixing and can greatly improve heat transfer within the channel. The analysis reveals a clear overall trend: increasing the Re leads to a stronger influence of the winglets on vortex formation. However, there seems to be a plateau in this effect. The differences in streamlines and vortex intensity become less noticeable between $Re=10000$ and $Re=16000$, particularly comparing the final cases ($Re=13000$ and $Re=16000$). This suggests that while increasing Re improves heat transfer initially, there are diminishing returns beyond a certain point. This trend is similar for other attack angles as well.

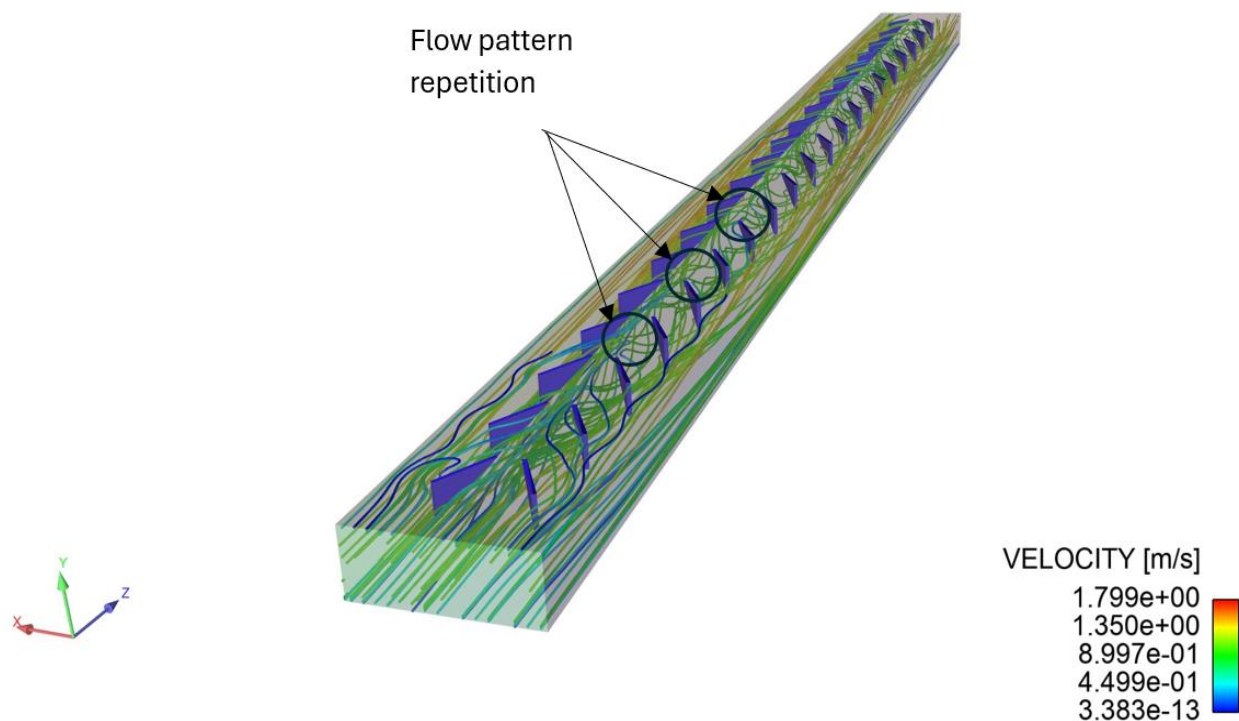


Figure 10. Flow Pattern Inside the Channel at $Re=3500$ and $\alpha=30^\circ$.

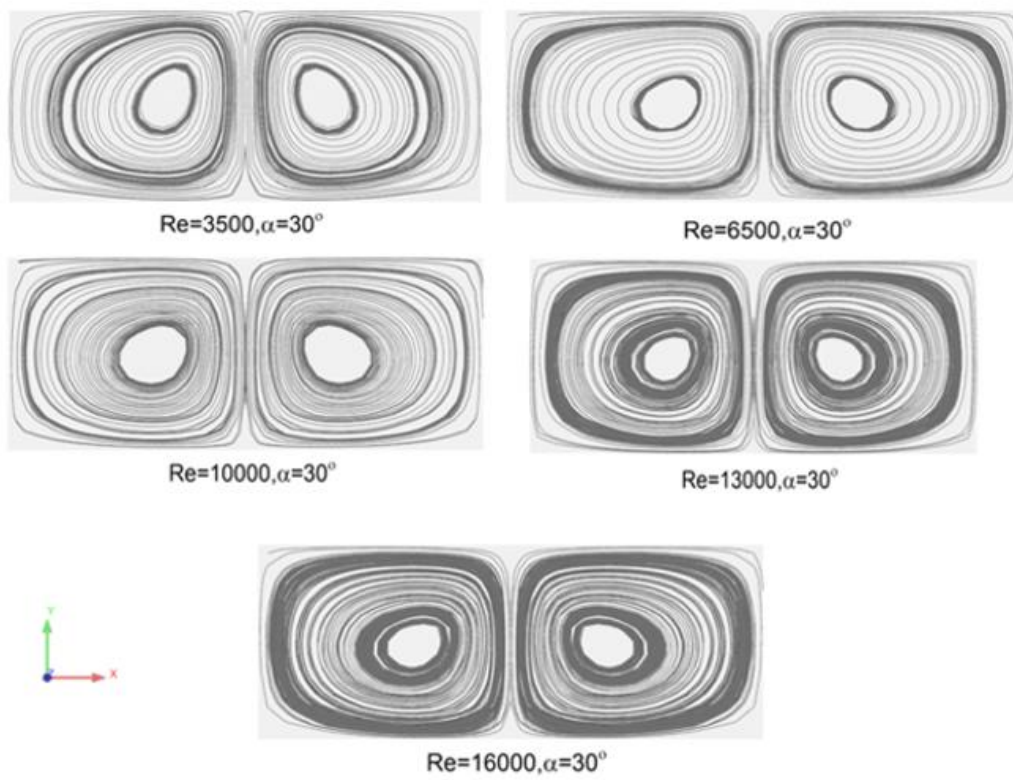


Figure 11. Details of Streamlines in Different Re .

Figure 12 shows variations in the transverse plane temperature distribution at a specific downstream distance ($z/L=0.531$) and Re of 6500. A visual representation of the absorber plate temperature is provided, where red indicates the highest temperatures and blue signifies the lowest temperatures. Red regions correspond to zones with lower heat transfer between the airflow and the absorber plate, hence they remain at a high temperature. Edge effects can also be seen where the temperature is higher in the middle of the duct and at its sides. As the angle of attack goes from 30° to 60° , it is noted that the temperature along the upper surface (absorber) begins to decrease which shows increasing heat transfer between the absorber and bulk flow, but then increases again as the angle of attack climbs from 60° to 90° . Furthermore, the results imply that the most effective fluid mixing occurs at an angle of attack of 60° , leading to the thinnest thermal boundary layer at the top, in contrast to the thicker region of temperature gradation at other angles of attack. Furthermore, at an angle of attack of 60° , there is very little temperature difference between the average temperature along the top surface and the average temperature across the whole transverse plane shown. These findings suggest that the convective heat transfer rate is higher at an angle of attack of 60° . These results are in agreement with the results of Wu et al. [31]. It is observed that the optimal convective heat transfer also occurs at an attack angle of 60° for a Re of 3500. However, for higher Re values (10000, 13000, and 16000), the optimal angle shifts to 45° .

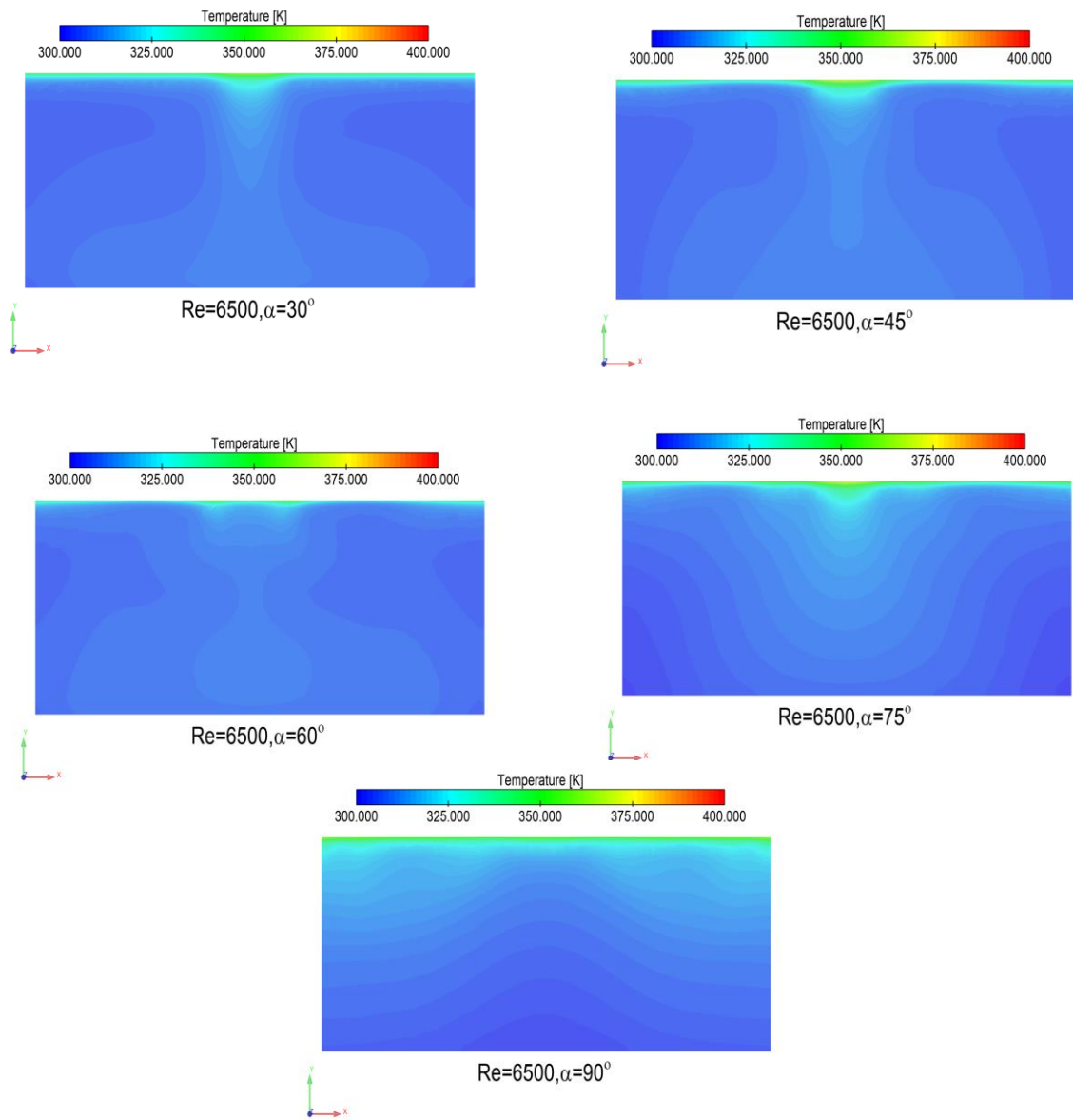


Figure 12. Temperature Field of Channel with Common Flow-up Delta Winglet Vortex Generator at $Re=6500$ and $z/L=0.531$.

Figure 13 illustrates the distribution of vorticity within the flow field for delta winglets at various attack angles (α) ranging from 30° to 90° . Vorticity, represented by the curl of velocity at various points in the fluid domain [4], signifies the rotational characteristic of the flow. In the figure, the colours further from green indicate higher vorticities with red being positive (counterclockwise) and blue being negative (clockwise). As evident from the figure, the flow exhibits the strongest vorticity magnitude at an attack angle of $\alpha=60^\circ$. Circulation starts at an attack angle of $\alpha=30^\circ$, and results in better air movement and in resulting better heat convection in the area. This pattern continues and reaches the highest improvement at $\alpha=60^\circ$ and disappears with higher attack angles. The strength of vorticity near the bottom and top walls of the SAH duct is also at its highest value at $\alpha=60^\circ$. While the strongest vorticity occurs at an attack angle of 60° for $Re=3500$ and

6500 (latter shown in Figure 13), this peak vorticity shifts to 45° for higher Re ($Re=10000$, 13000 , and 16000).

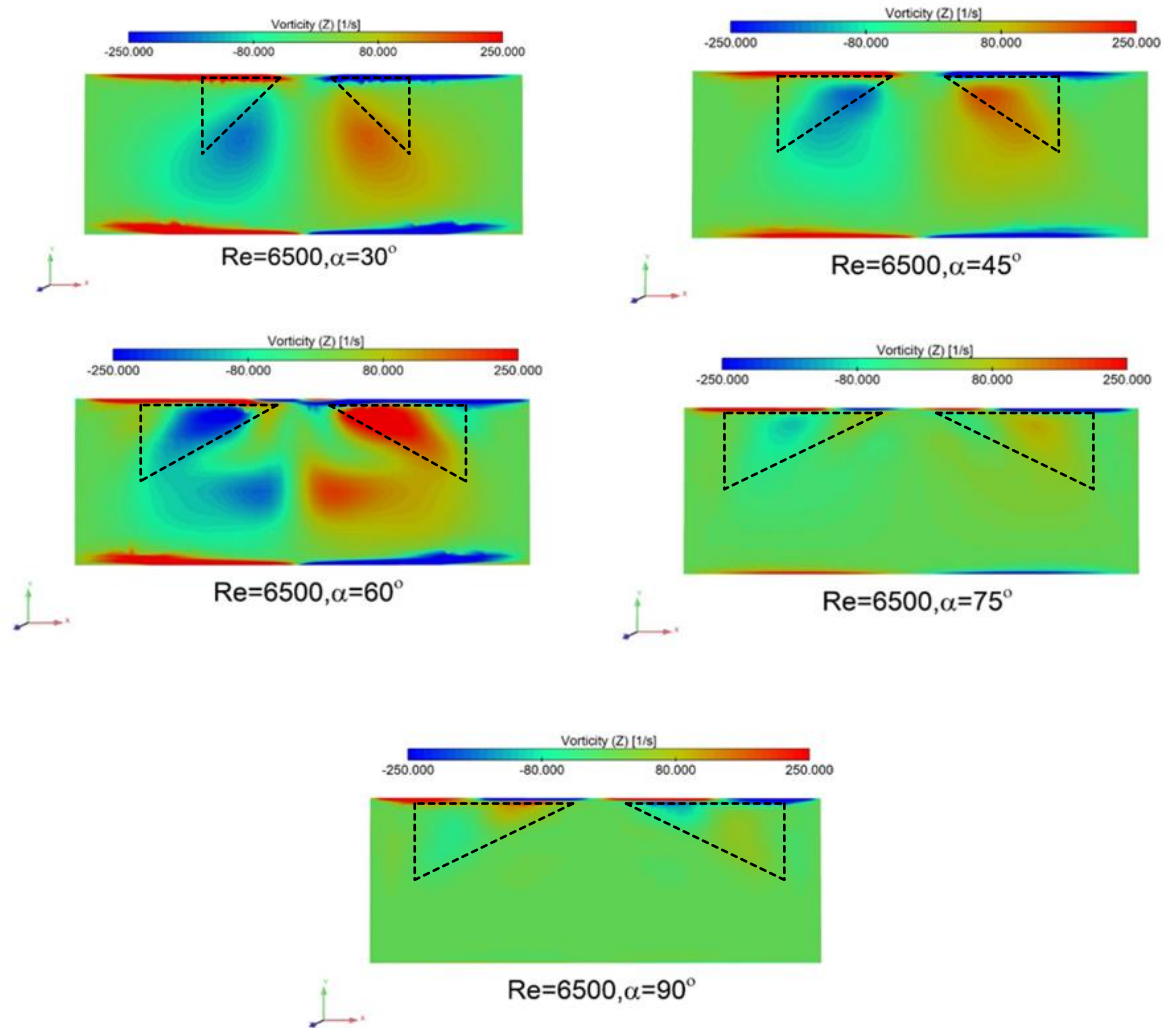


Figure 13. Vorticity Contour, for $Re=6500$ at Attack Angles of 30° , 45° , 60° , 75° , 90° and $z/L=0.531$.

The movement of vorticities' downstream can be better observed in Figure 14. At a Re of 6500, the vortex structures generated by delta winglets at a 60° attack angle demonstrate a strong interaction as they propagate downstream. This interaction between vortices enhances mixing within the flow, promoting superior heat transfer. This figure only shows cells where the absolute value of vorticity is 100.

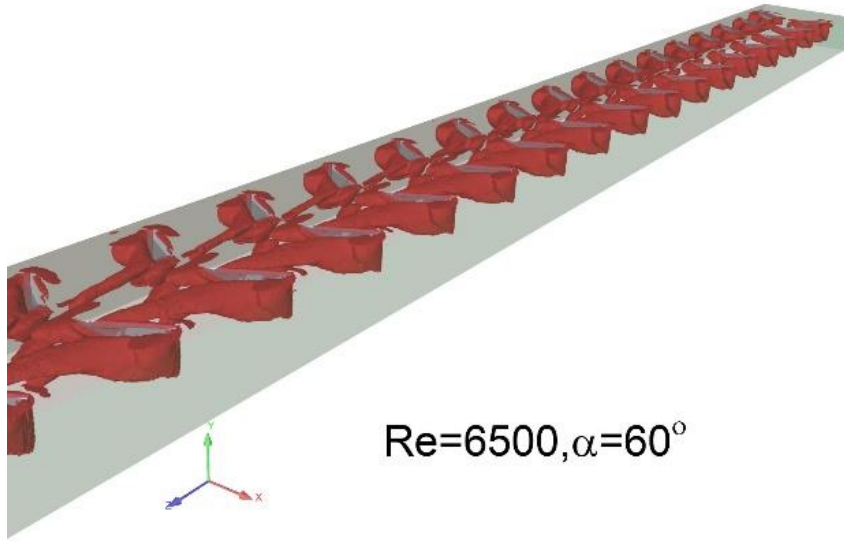


Figure 14. Iso Vortex Downstream of SAH for $Re=6500$, Attack Angle of 60° .

4.4 Nusselt number and friction factor correlations

To effectively analyze the combined impact of Re and attack angle, on heat transfer and flow resistance, correlations for the Nu and friction factor were established. These correlations were derived through multivariate nonlinear regression, providing a mathematical relationship between Nu or f and Re , and α . The specific design parameters incorporated into the analysis were $\alpha=30^\circ$, 45° , 60° , 75° , and 90° and Re ranging from 3500 to 16000. The final correlations, representing the outcome of the regression analysis [19], are provided below:

$$Nu = -16.13 + 7.22 \times 10^{-3} \times Re + 1.55 \times \alpha - 8.44 \times 10^{-8} \times Re^2 - 1.36 \times 10^{-2} \times \alpha^2 - 2.15 \times 10^{-5} \times (Re \times \alpha) \quad (14)$$

$$f = -0.06 - 4.42 \times 10^{-6} \times Re + 0.01 \times \alpha + 1.60 \times 10^{-10} \times Re^2 - 4.5 \times 10^{-5} \times \alpha^2 - 6.50 \times 10^{-9} \times (Re \times \alpha) \quad (15)$$

Primarily, Figure 15 shows that using formula (14) on (15) to predict Nu and f does a good job because the slope of the line is 1, and not many points fall outside the 95% confidence limit.

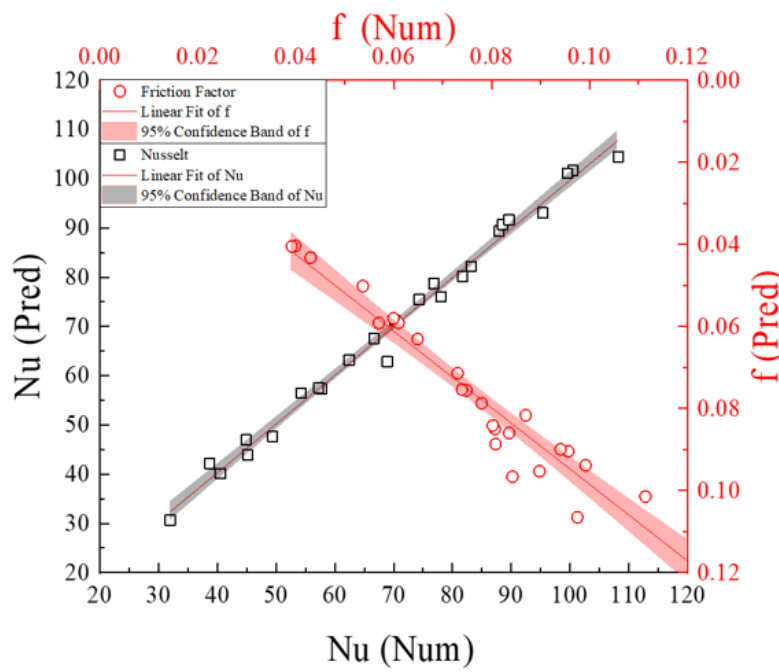


Figure 15. Predicted Nu and f (Pred) Versus Data from Simulation (Num).

The calculated R-squared value for Nu is 0.9902, indicating that 99.02% of the variation in the simulated Nu values can be explained by the correlation model. This suggests that the correlation accurately predicts the Nu values for different combinations of Reynolds number and attack angle.

For the friction factor, the R-squared value is 0.8024, indicating that 80.24% of the variation in the simulated f values can be explained by the correlation model. While this is a strong correlation, it suggests that there might be other factors influencing the friction factor that are not captured by the current model.

Figure 16(a) demonstrates a positive correlation between the Nu and the Re across all investigated attack angles (30° , 45° , 60° , 75° , and 90°). Interestingly, the attack angle corresponding to the maximum Nu value shifts with the changing Re . For $Re=3500$ and 6500 , the highest Nu is observed at a 60° attack angle, but this transitions to 45° for higher Re ($Re=10000$, 13000 , and 16000). Furthermore, Figure 16(b) shows the ratio of Nu for the winglet-equipped channels to the Nu of a smooth channel at the same Re exhibits a decreasing trend with increasing Re for all attack angles. This implies that the greatest enhancements in heat transfer relative to a smooth channel occurs at the lowest Re value (3500) which are 2.8, 3.0, 3.2, 2.5, and 2.0 at attack angles of 30° , 45° , 60° , 75° , 90° , respectively. Across the tested attack angles (30° to 90°), for Re of 3500 and 6500 , the Nu increases as the attack angle increases from 30° to 60° , but then decreases as the angle approaches 90° . This indicates a peak heat transfer

performance at an attack angle of 60° within this Re range. At higher Re ($Re=10000$, 13000 , 16000), the optimal attack angle for maximizing the Nu shifts to 45° .

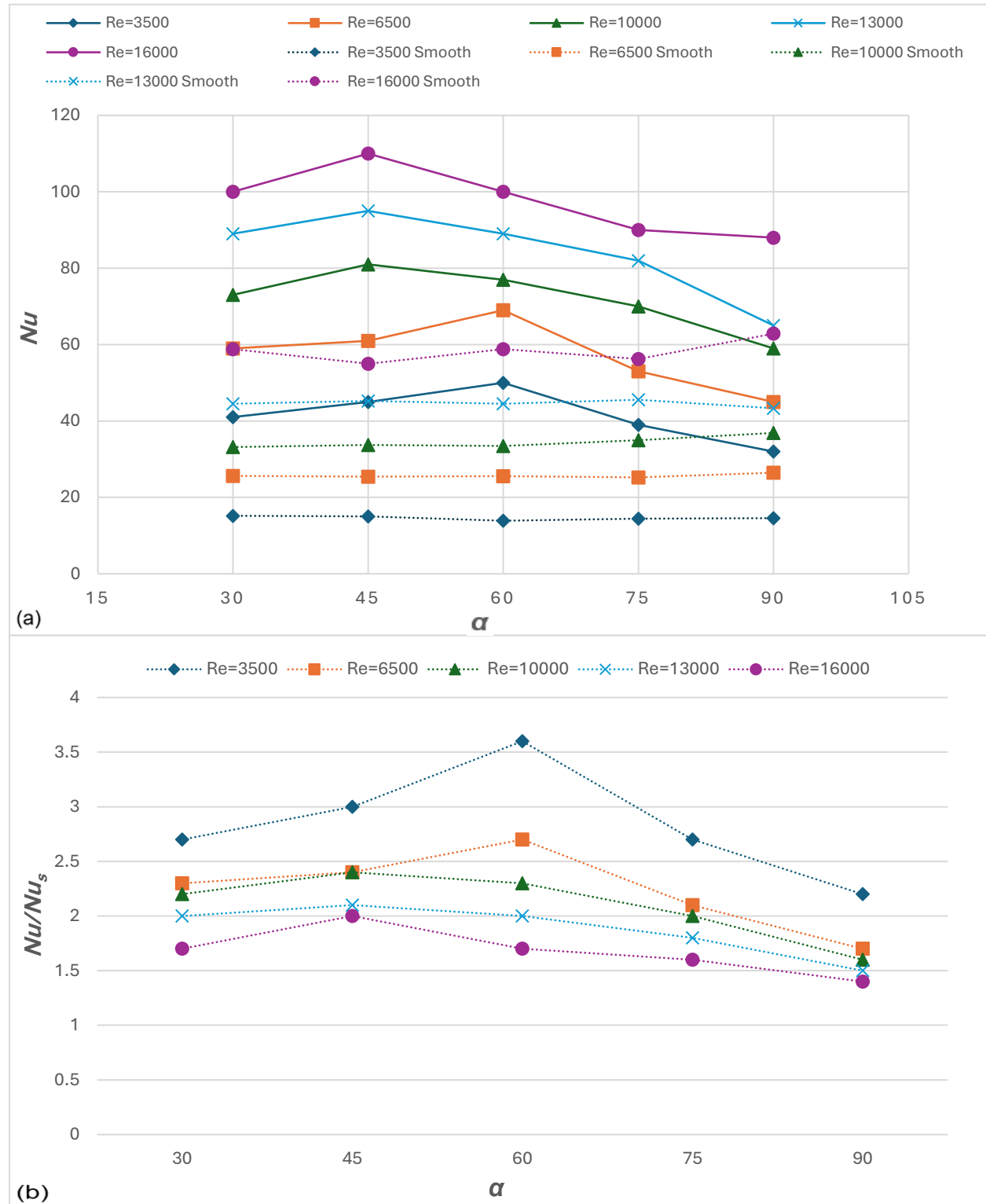


Figure 16. Influence of Angle of Attack on Nu in Different Flow Regimes a) Nusselt Number of the Duct with Winglets, and b) Nusselt Number Scaled to the Case of Smooth Channel.

Finally, as it is shown in Figure 17(a), the friction factor decreases consistently with increasing Re for all attack angles investigated. This implies that the lowest friction factor is for attack angle of 30° at Re 16000. Investigating the enhancement in friction factor relative to a smooth channel, Figure 17(b), The normalized friction factor initially decreases as the Re increases from 3500 to 6500. Subsequently, it exhibits a gradual, continuous increase at higher Re .

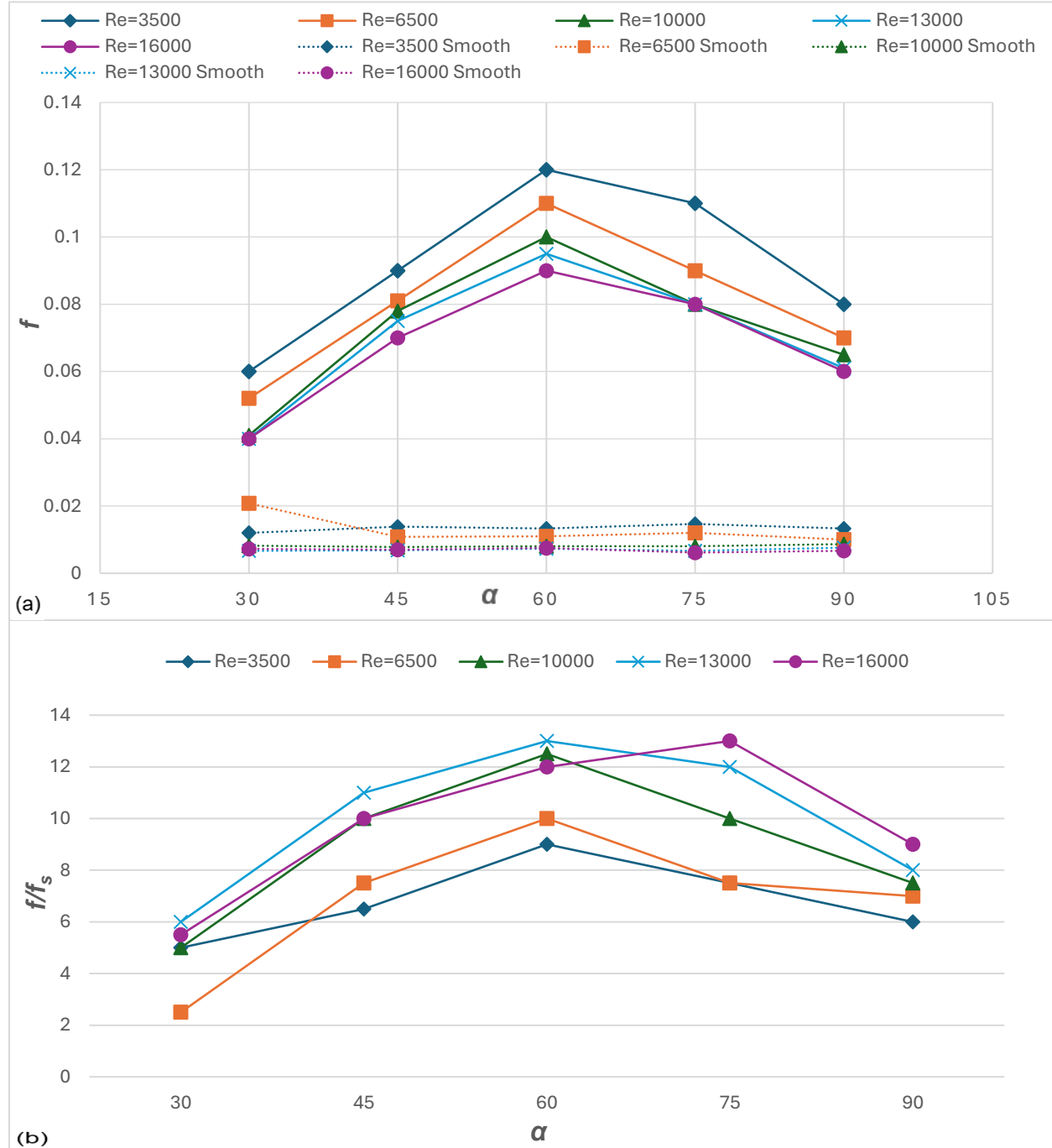


Figure 17. Influence of Angle of Attack on f in Different Flow Regimes a) f of the Duct with Winglets, and b) f Scaled to the Case of Smooth Channel.

The overarching goal is to optimize the thermal efficiency factor, TEF , which accounts for both heat transfer enhancement (represented by the normalized Nu) and the associated increase in flow resistance (represented by the normalized friction factor). Figure 18 reveals that the highest TEF value (1.7) is achieved at a Re of 3500 and an attack angle of 30° . Furthermore, a clear trend emerges; the TEF decreases as the Re increases across all investigated attack angles. In fact, at the highest Re , the use of a common flow-up WVGs decreases the TEF at all attack angles. This observation suggests that at higher Re , the pre-existing flow turbulence diminishes the relative impact of winglets on heat transfer enhancement. However, the winglets continue to introduce additional drag, leading to an increase in the friction factor.

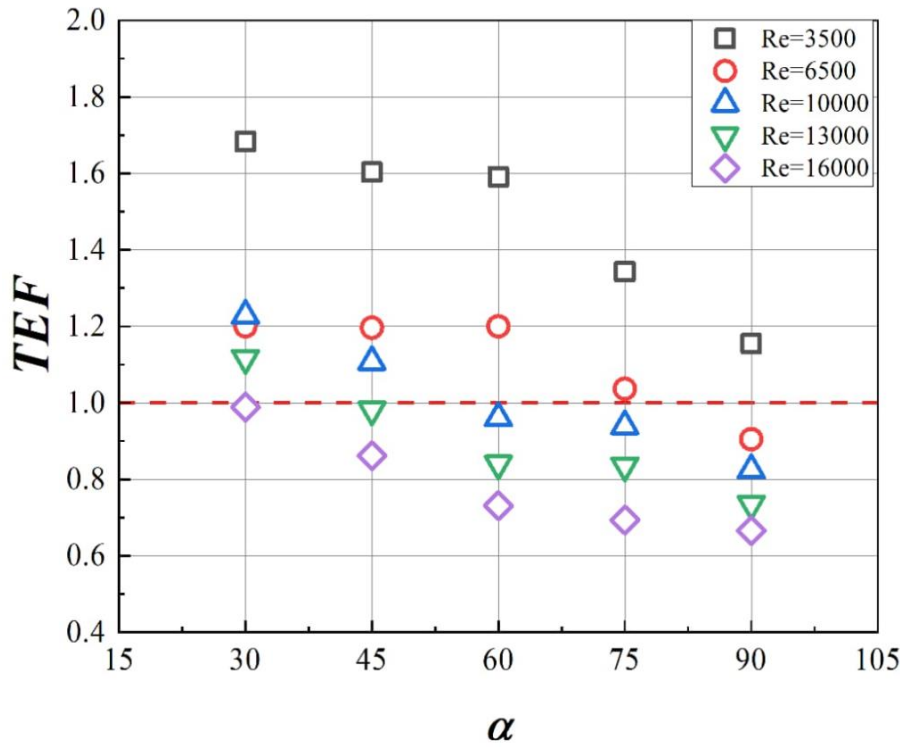


Figure 18. Influence of α and Re on Thermal Efficiency Factor.

This study and Chamoli et al. [19] both found a positive correlation between the Nu and the Re , indicating that heat transfer performance improves at higher flow rates. This trend was observed across all investigated attack angles. However, there are notable differences in the specific values observed. Chamoli et al. [19] reported a maximum Nu of 180 at an attack angle of 60° and Re of 16000. In the present study, the maximum Nu reached only 110. Similarly, the maximum friction factor was 0.1351 in Chamoli et al.'s [19] study (at an attack angle of 60° and Re 3500), compared to a lower value of 0.12 observed in the present study. Consequently, the thermal efficiency factor

also exhibited a difference in range, with Chamoli et al. reporting values between 1.17 and 2.2, while the present study found a *TEF* range of 0.75 to 1.7.

The differences in maximum *Nu*, friction factor, and *TEF* likely result from common flow-up winglet arrangement, (where Chamoli et al.'s studied common flow-down). This suggests that the common flow-down is a more efficient configuration for improving heat transfer. These results emphasize the significant influence that winglet configuration and flow conditions have on solar air heater (SAH) performance. Notably, Ke et al. [38] reported superior overall performance of common flow-up winglets compared to common flow-down within the *Re* range of <2200 and an attack angle of 45°, which can be the result of lower *Re* numbers applied to this study.

In the study by Chamoli et al. [19], the highest Nusselt number ratio $\frac{Nu}{Nu_s}$ of 4.2 and friction factor ratio $\frac{f}{f_s}$ of 10 were achieved at an attack angle of 30° and a Reynolds number of 3500. In contrast, the present study, also conducted at the same attack angle and Reynolds number, yielded a $\frac{Nu}{Nu_s}$ of 2.8 and $\frac{f}{f_s}$ of 5. Although Chamoli et al. [19] observed a higher friction factor, their overall thermal enhancement factor was also higher, indicating a more favorable balance between heat transfer enhancement and pressure drop penalty. Specifically, transitioning from the common flow-down to the common flow-up configuration resulted in a decrease in the Nu/Nu_s ratio by a factor of 1.5 and a decrease in the f/f_s ratio by a factor of 2. This suggests that the specific winglet configuration and arrangement used in Chamoli et al. [19] might be more effective in achieving a higher *TEF* despite the increased friction.

5. CONCLUSION AND FUTURE DIRECTIONS

5.1 Conclusions

This numerical study explored how adding winglet vortex generators (WVGs) to a SAH changes its heat transfer and airflow properties under different flow rates (Re number=3500, 6500, 10000, 13500, 16000) and angles of attack ($\alpha=30^\circ$, 45° , 60° , 75° , and 90°) with common flow-up arrangement of winglets compared to a smooth channel.

- Nu in a common flow-up arrangement of WVGs increased with an increase in Re Number. The presence of vortex generators with $\alpha=60^\circ$ at $Re=3500$ leads to strong vortices and as a result, heat transfer rate increases 3.6 times over the smooth channel.
- $\frac{Nu}{Nu_s}$ and $\frac{f}{f_s}$ increase with the initial increase in the attack angle from 30° to 60° , and then decrease from 60° to 90° . $\frac{Nu}{Nu_s}$ is 2.6, 3.1 and 2 for 30° , 60° , 90° , respectively and $\frac{f}{f_s}$ is 4.9, 9 and 6.2 for 30° , 60° , 90° , respectively.
- The TEF in the SAH equipped with WVGs decreases with increasing Re . The maximum TEF reached 1.7 at attack angle of 30° , and $Re=3500$.
- While the insertion of winglet vortex generators demonstrates clear potential for enhancing solar air heater performance, the optimal thermal efficiency factor remains dependent on specific design parameters and flow conditions. Chamoli et al. [19] achieved a maximum TEF of approximately 2.20 with a common flow-down arrangement, an attack angle of 30 degrees ($\alpha=30^\circ$), and at a Re of 3500. In the present study, the highest TEF achieved (1.7) occurred within a common flow-up arrangement, indicating the influence of these geometric design choices on SAH performance.

5.2 Future Research Directions

- **Solar Radiation Modeling:** The current study utilizes a simplified model of solar radiation by representing it as a uniform, constant heat flux boundary condition. To achieve even greater realism in future investigations, it would be beneficial to incorporate a more nuanced model that simulates the time-varying and directional nature of real-world solar radiation. This could potentially impact the temperature distribution on the absorber plate and influence the performance of winglets.
- **Experimental Validation:** While the present study relies on numerical simulations, conducting experimental work in the future is crucial. Experimental results will provide

valuable validation for the correlations developed for the Nu and friction factor. This validation step will strengthen the confidence in the models and their ability to predict solar air heater performance accurately.

REFERENCES

- [1] G. N. Tiwari, J. K. Yadav, D. B. Singh, I. M. Al-Helal, and A. M. Abdel-Ghany, "Exergoeconomic and enviroeconomic analyses of partially covered photovoltaic flat plate collector active solar distillation system," *Desalination*, vol. 367, pp. 186-196, 2015, doi: 10.1016/j.desal.2015.04.010.
- [2] P. Promvonge, P. Promthaisong, and S. Skullong, "Numerical heat transfer in a solar air heater duct with punched delta-winglet vortex generators," *Case Studies in Thermal Engineering*, vol. 26, Article 101088, 2021, doi: 10.1016/j.csite.2021.
- [3] M. R. Ali, K. Al-Khaled, M. Hussain, R. sadat., "Effect of design parameters on passive control of heat transfer enhancement phenomenon in heat exchangers—A brief review," *Case Studies in Thermal Engineering*, vol. 43, Article 102674, 2023, doi: 10.1016/j.csite.2022.
- [4] C. M. Jubayer, K. Siddiqui, and H. Hangan, "CFD analysis of convective heat transfer from ground mounted solar panels," *Solar Energy*, vol. 133, pp. 556-566, 2016, doi: 10.1016/j.solener.2016.04.027.
- [5] A. T. Wijayanta, I. Yaningsih, M. Aziz, T. Miyazaki, and S. Koyama, "Double-sided delta-wing tape inserts to enhance convective heat transfer and fluid flow characteristics of a double-pipe heat exchanger," *Appl Therm Eng*, vol. 145, pp. 27-37, 2018, doi: 10.1016/j.applthermaleng.2018.09.009.
- [6] A. S. Yadav, S. Gupta, A. Agrawal, R. Saxena, N. Agrawal, and S. Nashine, "Performance enhancement of solar air heater by attaching artificial rib roughness on the absorber Plate," *Mater Today Proc*, vol. 63, pp. 706-717, 2022, doi: 10.1016/j.matpr.2022.05.064.
- [7] A. F. Ismail, A. S. A. Hamid, A. Ibrahim, H. Jarimi, and K. Sopian, "Performance analysis of a double pass solar air thermal collector with porous media using lava rock," *Energies (Basel)*, vol. 15, no. 3, Article en15030905, 2022, doi: 10.3390.
- [8] S. Yari, H. Safarzadeh, and M. Bahiraei, "Experimental study of storage system of a solar water heater equipped with an innovative absorber spherical double-walled tank immersed in a phase change material," *J Energy Storage*, vol. 61, Article 106782, 2023, doi: 10.1016/j.est.2023.
- [9] C. Ramesh, S. Viajayakumar, S. Alshahrani, H. Panchal, "Performance enhancement of selective layer coated on solar absorber panel with reflector for water heater by response surface method: A case study," *Case Studies in Thermal Engineering*, vol. 36, Article 102093, 2022, doi: 10.1016/j.csite.2022.
- [10] S. K. Mohanakrishnan, Y. Yang, D. S. K. Ting, and S. Ray, "The effect of transverse spacing of a winglet pair on flat plate heat convection," *Appl Therm Eng*, vol. 194, Article 117094, 2021, doi: 10.1016/j.applthermaleng.2021.
- [11] A. Kumar and A. Layek, "Evaluation of the performance analysis of an improved solar air heater with Winglet shaped ribs," *Experimental Heat Transfer*, vol. 35, no. 3, pp. 239-257, 2022, doi: 10.1080/08916152.2020.1838670.

- [12] A. O. Alsaieri, H. A. H. Alzahrani, N. Madhukeshwara, and B. M. Prasanna, "Heat transfer augmentation in a solar air heater with conical roughness elements on the absorber," *Case Studies in Thermal Engineering*, vol. 36, Article 102210, 2022, doi: 10.1016/j.csite.2022.
- [13] K. S. Mushatet and N. M. Bader, "experimental investigation for the performance of the solar air dryer with vortex generator," *Defect and Diffusion Forum*, vol. 419, pp. 57-67, 2022, doi: 10.4028/p-a8x5o3.
- [14] G. N. Tiwari, *Solar Energy Fundamentals, Design, Modelling and Applications*. 2002. Narosa; 1st edition (May 22 2002)
- [15] Hottel H.C., Woertz B.B. "Performance of a flat-plate solar heat collector," *Solar Energy*, vol. 1, no. 1, pp. 63-68, 1957, doi: 10.1016/0038-092x(57)90091-9.
- [16] S. A. Kalogirou, "Solar thermal collectors and applications," *Progress in Energy and Combustion Science*, vol. 30, no. 3, pp. 231-295, 2004. doi: 10.1016/j.pecs.2004.02.001.
- [17] J. A. Duffie and W. A. Beckman, *Solar Engineering of Thermal Processes*. 4th ed. John Wiley and Sons. 2013.
- [18] M. A. Karim and M. N. A. Hawlader, "Performance investigation of flat plate, v-corrugated and finned air collectors," *Energy*, vol. 31, no. 4, pp. 452-470, 2006, doi: 10.1016/j.energy.2005.03.007.
- [19] S. Chamoli, R. Lu, D. Xu, and P. Yu, "Thermal performance improvement of a solar air heater fitted with winglet vortex generators," *Solar Energy*, vol. 159, pp. 966-983, 2018, doi: 10.1016/j.solener.2017.11.046.
- [20] A. Bekele, M. Mishra, and S. Dutta, "Heat transfer augmentation in solar air heater using delta-shaped obstacles mounted on the absorber plate," *International Journal of Sustainable Energy*, vol. 32, no. 1, pp. 53-69, 2013, doi: 10.1080/14786451.2011.598637.
- [21] A. Kumar, R. P. Saini, and J. S. Saini, "Development of correlations for Nusselt number and friction factor for solar air heater with roughened duct having multi V-shaped with gap rib as artificial roughness," *Renew Energy*, vol. 58, pp. 151-163, 2013, doi: 10.1016/j.renene.2013.03.013.
- [22] N. K. Pandey, V. K. Bajpai, and Varun, "Experimental investigation of heat transfer augmentation using multiple arcs with gap on absorber plate of solar air heater," *Solar Energy*, vol. 134, pp. 314-326, 2016, doi: 10.1016/j.solener.2016.05.007.
- [23] S. Tamna, S. Skullong, C. Thianpong, and P. Promvonge, "Heat transfer behaviors in a solar air heater channel with multiple V-baffle vortex generators," *Solar Energy*, vol. 110, pp. 720-735, 2014, doi: 10.1016/j.solener.2014.10.020.
- [24] S. Skullong, P. Promvonge, C. Thianpong, and M. Pimsarn, "Thermal performance in solar air heater channel with combined wavy-groove and perforated-delta wing vortex generators," *Appl Therm Eng*, vol. 100, pp. 614-620, 2016, doi: 10.1016/j.applthermaleng.2016.01.107.
- [25] G. Lu and G. Zhou, "Numerical simulation on performances of plane and curved winglet type vortex generator pairs with punched holes," *Int J Heat Mass Transf*, vol. 102, pp. 679-690, 2016, doi: 10.1016/j.ijheatmasstransfer.2016.06.063.

- [26] A. Kumar and A. Layek, "Energetic and exergetic performance evaluation of solar air heater with twisted rib roughness on absorber plate," *J Clean Prod*, vol. 232, pp. 617-628, 2019, doi: 10.1016/j.jclepro.2019.05.363.
- [27] P. Promvonge, N. Koolnapadol, M. Pimsarn, and C. Thianpong, "Thermal performance enhancement in a heat exchanger tube fitted with inclined vortex rings," *Appl Therm Eng*, vol. 62, no. 1, pp. 285-292, 2014, doi: 10.1016/j.applthermaleng.2013.09.031.
- [28] S. R. Hiravennavar, E. G. Tulapurkara, and G. Biswas, "A note on the flow and heat transfer enhancement in a channel with built-in winglet pair," *Int J Heat Fluid Flow*, vol. 28, no. 2, pp. 299-305, 2007, doi: 10.1016/j.ijheatfluidflow.2006.03.030.
- [29] M. A. Althaher, A. A. Abdul-Rassol, H. E. Ahmed, and H. A. Mohammed, "Turbulent heat transfer enhancement in a triangular duct using delta-winglet vortex generators," *Heat Transfer - Asian Research*, vol. 41, no. 1, pp. 43-62, 2012, doi: 10.1002/htj.20382.
- [30] L. H. Tang, W. X. Chu, N. Ahmed, and M. Zeng, "A new configuration of winglet longitudinal vortex generator to enhance heat transfer in a rectangular channel," *Appl Therm Eng*, vol. 104, pp. 74-84, 2016, doi: 10.1016/j.applthermaleng.2016.05.056.
- [31] H. Wu, D. S. K. Ting, and S. Ray, "The effect of delta winglet attack angle on the heat transfer performance of a flat surface," *Int J Heat Mass Transf*, vol. 120, pp. 117-126, 2018, doi: 10.1016/j.ijheatmasstransfer.2017.12.030.
- [32] S. Caliskan, "Experimental investigation of heat transfer in a channel with new winglet-type vortex generators," *Int J Heat Mass Transf*, vol. 78, pp. 604-614, 2014, doi: 10.1016/j.ijheatmasstransfer.2014.07.043.
- [33] R. Karwa and B. K. Maheshwari, "Heat transfer and friction in an asymmetrically heated rectangular duct with half and fully perforated baffles at different pitches," *International Communications in Heat and Mass Transfer*, vol. 36, no. 3, pp. 264-268, 2009, doi: 10.1016/j.icheatmasstransfer.2008.11.005.
- [34] S. Skullong and P. Promvonge, "Experimental investigation on turbulent convection in solar air heater channel fitted with delta winglet vortex generator," *Chin J Chem Eng*, vol. 22, no. 1, pp. 1-10, 2014, doi: 10.1016/S1004-9541(14)60030-6.
- [35] J. Min and B. Zhang, "Convective mass transfer enhancement in a membrane channel by delta winglets and their comparison with rectangular winglets," *Chin J Chem Eng*, vol. 23, no. 11, pp. 1755-1762, 2015, doi: 10.1016/j.cjche.2015.09.006.
- [36] T. Alam and M. H. Kim, "Numerical study on thermal hydraulic performance improvement in solar air heater duct with semi-ellipse shaped obstacles," *Energy*, vol. 112, pp. 588-598, 2016, doi: 10.1016/j.energy.2016.06.105.
- [37] R. Karwa, R. D. Bairwa, B. P. Jain, and N. Karwa, "Experimental study of the effects of rib angle and discretization on heat transfer and friction in an asymmetrically heated rectangular duct," *Journal of Enhanced Heat Transfer*, vol. 12, no. 4, pp. 345-355, 2005, doi: 10.1615/JEnhHeatTransf.v12.i4.40.
- [38] Z. Ke, C. L. Chen, K. Li, S. Wang, and C. H. Chen, "Vortex dynamics and heat transfer of longitudinal vortex generators in a rectangular channel," *Int J Heat Mass Transf*, vol. 132, pp. 871-885, 2019, doi: 10.1016/j.ijheatmasstransfer.2018.12.064.

- [39] S. Chamoli, N. S. Thakur, and J. S. Saini, "A review of turbulence promoters used in solar thermal systems," *Renewable and Sustainable Energy Reviews*, vol. 16, no. 5, pp. 3154-3175, 2012. doi: 10.1016/j.rser.2012.01.021.
- [40] G. Zhou and Q. Ye, "Experimental investigations of thermal and flow characteristics of curved trapezoidal winglet type vortex generators," *Appl Therm Eng*, vol. 37, pp. 241-248, 2012, doi: 10.1016/j.applthermaleng.2011.11.024.
- [41] P. J. Boache, "Perspective: A method for uniform reporting of grid refinement studies," *Journal of Fluids Engineering, Transactions of the ASME*, vol. 116, no. 3, pp. 405-413, 1994, doi: 10.1115/1.2910291.

VITA AUCTORIS

NAME: Mehrnaz Mehdizadeh Farsangi

PLACE OF BIRTH: Kerman, Iran

YEAR OF BIRTH: 1994

EDUCATION: Shahid Rezvani nejad Highschool, Kerman, Iran
2008-2012

Shahid Bahonar University of Kerman, Kerman, Iran
2012-2017, B.Sc.

University of Windsor, Windsor, Canada
2022-2024, M.Sc.